

## CHAPTER 1

# *An Introduction to Motility-Induced Phase Separation*

JÉRÉMY O'BYRNE<sup>a</sup>, ALEXANDRE SOLON<sup>b</sup>, JULIEN TAILLEUR<sup>a,\*</sup>,  
YONGFENG ZHAO<sup>c</sup>

<sup>a</sup>Université de Paris, Laboratoire Matière et Systèmes Complexes (MSC), UMR 7057 CNRS, F-75205 Paris, France, <sup>b</sup>Sorbonne Université, CNRS, Laboratoire Physique Théorique de la Matière Condensée, 75005 Paris, France, <sup>c</sup> Center for Soft Condensed Matter Physics and Interdisciplinary Research & School of Physical Science and Technology, Soochow University, 215006 Suzhou, China

\*corresponding email address: [julien.tailleur@univ-paris-diderot.fr](mailto:julien.tailleur@univ-paris-diderot.fr)

**Abstract.** Active particles may undergo phase separation when interactions oppose self-propulsion, in the absence of any cohesive forces. The corresponding Motility-Induced Phase Separation (MIPS) is arguably the simplest non-trivial collective feature that distinguishes active from passive particles. It is observed in a large variety of systems which we review in this chapter. We describe in depth the case of motile particles interacting via quorum-sensing interactions, whose theoretical framework is by now well-established. We close the chapter by discussing the features observed in systems undergoing MIPS that still challenge our understanding.

## Contents

---

<b>1.1</b>	<b>Introduction</b>	2
<b>1.2</b>	<b>Phenomenology</b>	4
<b>1.3</b>	<b>Position-dependent propulsion speed and mean-field instability towards MIPS</b>	7
<b>1.4</b>	<b>Large-scale long-time description in the presence of position-dependent propulsion speed</b>	9
1.4.1	A Fokker-Planck approximation	9
1.4.2	Fluctuating hydrodynamics	11
<b>1.5</b>	<b>Fluctuating hydrodynamics of Active Particles interacting via Quorum-Sensing (QSAPs)</b>	13
<b>1.6</b>	<b>Generalized thermodynamics of QSAPs</b>	15
1.6.1	The local approximation: an equilibrium theory	16
1.6.2	Gradient expansion: beyond the local approximation	20
1.6.3	The fully non-local theory	22
1.6.4	QSAPs: conclusion	23
<b>1.7</b>	<b>Active particles interacting via pairwise forces</b>	23
1.7.1	A quorum-sensing approximation	24
1.7.2	The stress tensor of PFAPs	25
1.7.3	MIPS in PFAPs: A mechanical instability	26
<b>1.8</b>	<b>MIPS in lattice models</b>	29
1.8.1	Models and phenomenology	29
1.8.2	Linear instability at mean-field level	29
<b>1.9</b>	<b>Conclusion</b>	32
<b>.1</b>	<b>Mean squared displacement of an RTP on lattice</b>	38
.1.1	Diffusivity	38
.1.2	Mean-square displacement at all times	39

---

## 1.1 Introduction

The liquid-gas phase separation of simple fluids is arguably the simplest phase transition encountered in equilibrium systems. Its microscopic origin can be understood from a simple inspection of the Boltzmann distribution. The latter implies that the most likely macroscopic state in which a system is found results from a competition between its entropy and its energy. In the presence of attractive interactions between the molecules, energy favours cohesion

---

Book Series: Soft Matter Science

*Out-of-Equilibrium Soft Matter: Active Fluids*

Edited by Luigi Gentile, Christina Kurzthaler and Howard A. Stone

© Royal Society of Chemistry 2020

Published by the Royal Society of Chemistry, [www.rsc.org](http://www.rsc.org)

whereas entropy favors disorder. The relative weights of entropy and energy in the steady state are controlled by temperature. When the latter is lowered, energy wins over entropy, promoting the emergence of a dense fluid phase over a gaseous state. When the total number of particles is conserved, this phase transition is replaced by phase coexistence.

Consider a microscopic model of attractively interacting particles in equilibrium. While the origin of its phase separation can be qualitatively accounted for by inspection of the Boltzmann weight, predicting any macroscopic property of the system starting from the microscopic level is a fantastic challenge. Instead, one rather coarse-grains the system to describe it at a mesoscopic level, using the so-called model B dynamics<sup>1</sup>

$$\frac{\partial}{\partial t} \rho(\mathbf{r}, t) = \nabla \cdot \left[ \Gamma_0 \nabla \frac{\delta \mathcal{F}[\rho]}{\delta \rho(\mathbf{r})} + \boldsymbol{\eta}(\mathbf{r}, t) \right] \quad (1.1)$$

where  $\mathcal{F}[\rho]$  is the free energy of the coarse-grained configuration  $\rho(\mathbf{r}, t)$ ,  $\Gamma_0$  is a mobility constant, and  $\boldsymbol{\eta}(\mathbf{r}, t)$  is a Gaussian white noise with variance  $\langle \eta_\alpha(\mathbf{r}', t') \eta_\beta(\mathbf{r}, t) \rangle = \Gamma_0 \delta_{\alpha\beta} \delta(t - t') \delta^d(\mathbf{r} - \mathbf{r}')$ . Equation (1.1) describes the evolution at late times and large scales of the order parameter of the system, here the density field of the fluid, and allows predicting the universal properties of equilibrium liquid-gas phase separation. Mean-field theories built out of Eq. (1.1) also accurately predict its phase diagram,<sup>2</sup> outside a Ginzburg interval around the critical point.

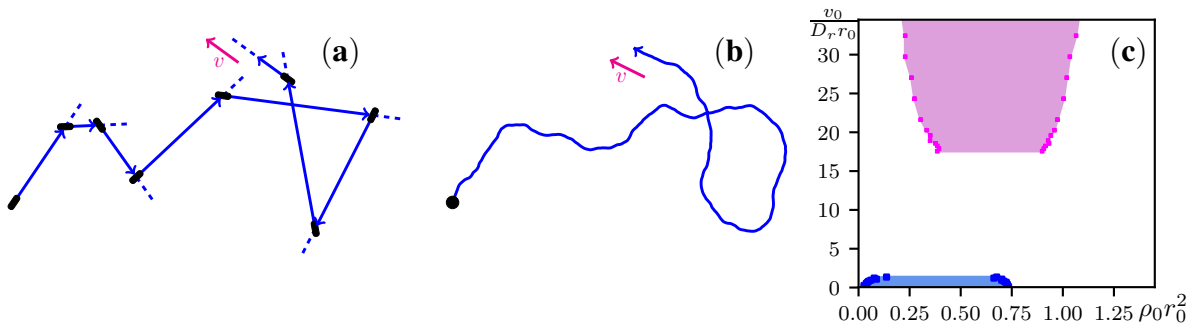


Figure 1.1: **(a)** Schematic trajectory of a Run-and-Tumble Particle (RTP). Runs in straight lines at fixed speed  $v$  are punctuated by tumbles, occurring with rate  $\alpha$ , during which the particle randomizes its orientation. **(b)** Schematic trajectory of an Active Brownian Particle (ABP). The orientation diffuses continuously, with a rotational diffusivity  $D_r$ . **(c)** Phase diagram of self-propelled ABPs interacting via a Lennard-Jones pair potential (See<sup>3</sup> for details of the model). The equilibrium phase-separated region (blue) survives for small enough self-propulsion speeds. Motility-induced phase separation (plum) is observed whenever the run-length  $v_0/D_r$  is significantly larger than 15 particle diameters  $r_0$ . Symbols correspond to coexisting densities.

In active matter, none of the tools described above are available to predict the phase behaviors of simple active fluids. Let us consider the persistent dynamics illustrated in Fig 1.1 which model the two-dimensional motion of bacteria and self-propelled colloids. A natural question is whether replacing the Brownian dynamics of passive colloids by such self-propelled dynamics completely alters the understanding of phase separation inherited from equilibrium physics. In the weak propulsion limit, or when attractive forces are strong enough to overcome self-propulsion ones, one expects the qualitative features of the passive case to survive.

At larger self-propulsion speeds, active forces are likely to overcome attractive ones, leading to homogeneous phases. Interestingly, Fig. 1.1 shows a richer picture. While phase-separation survives in the weak-self-propulsion, near-equilibrium regime, it is mostly observed far from it, when the persistence length of the particles is much larger than their individual size. Even more surprisingly, this phase separation would also be observed in the complete absence of attractive interactions. The underlying mechanism, known as motility-induced phase separation<sup>4</sup> (MIPS), is the topic of this chapter.

In Section 1.2, we start by reviewing the variety of systems in which MIPS has been reported. In Section 1.3, we show that it emerges from an instability due to a simple feedback mechanism. First, active particles generically accumulate where they go slower. Consequently, when interactions make active particles slow down at high density, they tend to accumulate where they are already denser than the average, hence making homogeneous phases unstable to density fluctuations. In Section 1.4, we demonstrate this tendency to accumulate in slower regions and characterize the large-scale long-times dynamics of active particles endowed with a non-uniform speed  $v(\mathbf{r})$ . The latter is then used in Section 1.5 to build a large-scale description of active particles interacting via quorum-sensing interactions. This theory can then be used to predict MIPS for this systems, and to characterize the corresponding phase diagram, which is the topic of Section 1.6. In Section 1.7, we then discuss the case of active particles interacting via pairwise forces, highlighting both similarities and differences with the case of quorum sensing. In Section 1.8, we finally discuss MIPS in lattice models. We close this chapter in Section 1.9 by discussing open problems and current research topics on MIPS.

## 1.2 Phenomenology

Let us first describe the types of systems that undergo MIPS. As we will show in the next sections, MIPS is triggered by a positive feedback loop: If interactions act to slow down the active particles, a small aggregate will accumulate more and more particles to ultimately lead to phase separation. Two types of interacting active particles have been shown, both in models and experiments, to experience such a slowdown leading to MIPS:

- *Quorum-Sensing Active Particles (QSAPs)*, which interact by adapting their velocity to the local density. Such quorum-sensing interactions are displayed, for example, by bacteria which may change their motility in response to the local concentration of a chemical that they release in the environment. This type of interaction, for which MIPS was first predicted,<sup>5</sup> is best amenable to analytic treatment. In particular, we will show in Sec. 1.5 that mesoscopic equations can be derived for such models using an adequate coarse graining procedure.
- *Pairwise-Forces Active Particles (PFAPs)* which interact via short-range pairwise repulsive interactions such as excluded volume interactions. Indeed, two active particles colliding head-to-head will stall each other until one of them either rotate or slide along the other. The speeds of the particles are thus reduced during the collision. When this effect is strong enough, it may trigger MIPS. This type of particles, discussed in more detail in Sec. 1.7, is harder to study analytically than QSAPs and offers a richer phenomenology, several aspects of which are still debated.

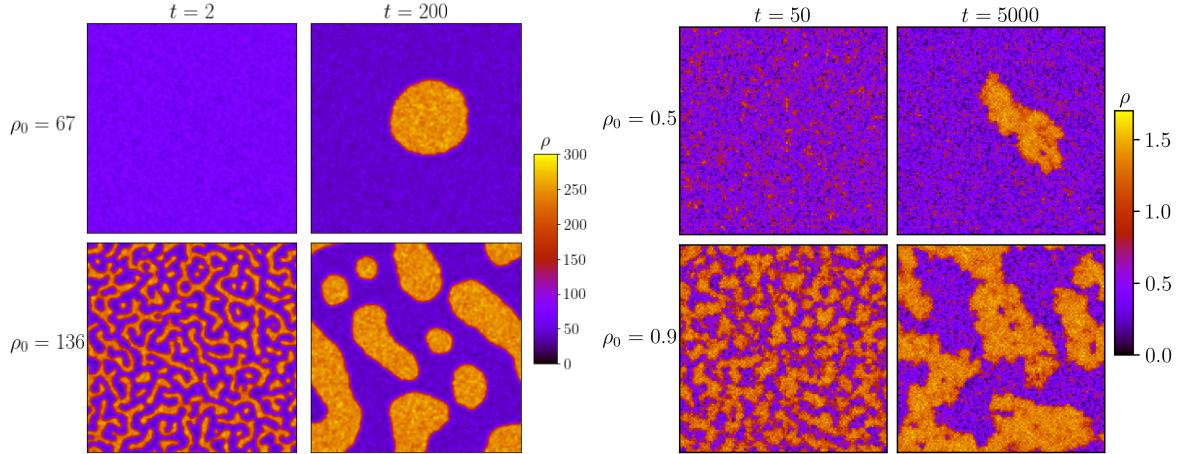


Figure 1.2: Nucleation (top rows) and spinodal decomposition (bottom rows). Left: QSAPs, see Fig. 1 of Ref.<sup>6</sup> for the details of the model. Right: PFAPs with the interaction potential  $V(r) = k(\sigma - r)^2\Theta(\sigma - r)$ ,  $k = 50$ ,  $\sigma = 1$ ,  $\nu = 5$ ,  $D_r = 0.2$ .

Both QSAPs and PFAPs come in different flavors corresponding to different dynamics of the self-propulsion velocity. Two common self-propulsion dynamics are shown in Fig. 1.1: Active Brownian particles (ABPs), which reorient continuously because of rotational noise, and run-and-Tumble Particles (RTPs), which “run” in straight lines between two “tumbles” during which they randomize their orientations. Active Ornstein-Uhlenbeck Particles (AOUPs)<sup>7,8</sup> are yet another kind of particles which have the interesting property of having Gaussian fluctuations of their self-propulsion velocity. Although the trajectories of these three particles seem markedly different, they all correspond to persistent random walks. All undergo MIPS and current knowledge suggests that these different active dynamics do not lead to important qualitative differences.<sup>8,9</sup>

In all these models, MIPS is observed with a phase diagram similar to the large velocity region of Fig. 1.1c. Between the two binodal lines, one observes a phase-separated steady state where a high density region comprising slowly moving particles coexists with a gaseous phase in which particles move more rapidly. Moreover, this coexistence state bears the hallmarks of liquid-gas phase separation that are spinodal decomposition, nucleation and metastability. Inside but close to the binodals, a homogeneous system is metastable until a large enough fluctuation nucleates a droplet and brings the system to a phase coexistence. On the contrary, between the spinodal lines, any homogeneous system is unstable to arbitrarily small fluctuations. One then observes spinodal decomposition: Starting from a homogeneous profile, many liquid or gas clusters are formed (depending on the majority phase), which then coarsen in time. Both phenomena are illustrated in Fig. 1.2.

Experimentally, MIPS has been investigated in different systems, either living (bacteria) or inert (self-propelled colloids). The most clear-cut realization of MIPS is arguably that of Ref.<sup>10</sup> which uses micrometric silica beads half-coated with carbon in a water-lutidine mixture. The activity of each particle is tuned in real time by using a laser focusing on the particles to adapt their velocities on the local density (see Fig. 1.3a), as for QSAPs *in silico*. This triggers MIPS, as shown in Fig. 1.3b. The same self-propelled colloids, when endowed with a uniform self-propulsion speed and interacting via pairwise repulsive forces, are found to form large clusters

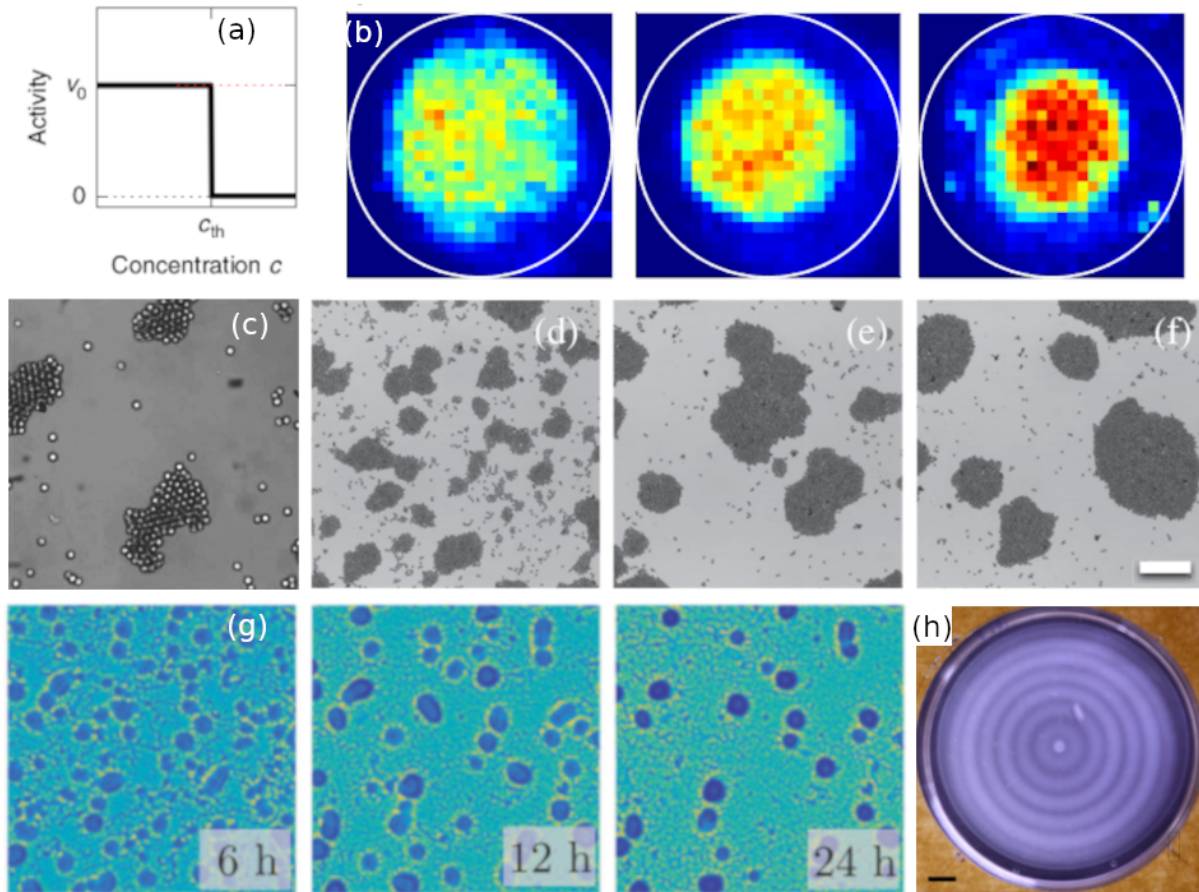


Figure 1.3: Experimental realizations of MIPS. (a,b) Self-propelled colloids whose motility is tuned by a computer-assisted loop to obtain the desired quorum-sensing interactions (a). One observes phase separation (b) with warmer colors denoting higher densities. The three snapshots correspond to three values of threshold concentration  $c_{th}$  increasing from left to right. (c) Self-propelled colloids interacting via pairwise repulsive forces. (d-f) Self-propelled colloids showing coarsening (d,e) up to a certain length scale (e,f) where MIPS is arrested because of alignment inside the clusters. (g) Formation of fruiting bodies for bacteria *Myxococcus xanthus*. (h) Arrested MIPS in genetically engineered *E. coli* bacteria where the population dynamics in the colony compete with MIPS to select a characteristic pattern size. Panel (a,b) are reproduced from Ref. <sup>10</sup> under the Creative Commons licence. Panel (c) is reproduced with permission from Ref. <sup>11</sup> DOI. [I. Buttinoni, J. Bialké, F. Kümmel, H. Löwen, C. Bechinger and T. Speck, Physical review letters, 110, 238301, 2013]. Copyright (2013) by the American Physical Society. Panel (d,f) are reproduced with permission from Ref. <sup>12</sup> DOI. [M. N. Van Der Linden, L. C. Alexander, D. G. Aarts and O. Dauchot, Physical review letters, 123, 098001, 2019]. Copyright (2019) by the American Physical Society. Panel (g) is reproduced with permission from Ref. <sup>13</sup> DOI. [G. Liu, A. Patch, F. Bahar, D. Yllanes, R. D. Welch, M. C. Marchetti, S. Thutupalli and J. W. Shaevitz, Physical review letters, 122, 248102, 2019]. Copyright (2019) by the American Physical Society. Panel (h) is courtesy of Prof Jian-Dong Huang.

(see Fig. 1.3c) that have also been described as an experimental realization of MIPS.<sup>11</sup>

In many other experimental systems, clustering or phase separation has been reported but a clear connection to MIPS proved elusive. First, additional ingredients may come in and arrest a *bona fide* MIPS. This is for instance the case for the titanium-coated Janus colloids that are self-propelled by an AC external electric field.<sup>12</sup> Phase separation is found to be arrested (see Fig. 1.3d,e,f), possibly because of the aligning interactions experienced by the colloids in the dense phase. Hydrodynamic<sup>14,15</sup> and phoretic<sup>16</sup> interactions have also been identified as potentially arresting MIPS in simulations. For the bacteria *Myxococcus xanthus*, it has been argued that MIPS leads to the formation of fruiting bodies which coarsen up to a certain size before other mechanisms become important (Fig. 1.3g).<sup>13</sup> Furthermore, in the bacteria that are genetically engineered to experience quorum-sensing interactions,<sup>17</sup> MIPS is arrested to a typical size because of the population dynamics of the bacteria,<sup>18</sup> thereby forming the alternating rings reproduced in Fig. 1.3h. Finally, in other systems, attractive interactions are known to play an important role. Janus self-diffusiophoretic colloids have been reported to exhibit phase-separation or clustering far outside the MIPS region.<sup>19–21</sup> Assessing the respective roles of MIPS and of attractive forces in these systems remains a challenge.

### 1.3 Position-dependent propulsion speed and mean-field instability towards MIPS

A first ingredient in the instability leading to MIPS is the propensity of active particles to accumulate where they move slower. To establish this fact, let us consider self-propelled particles with an isotropic reorientation mechanism and a self propulsion speed that is position dependent:  $\dot{\mathbf{r}} = v(\mathbf{r})\mathbf{u}$ . The master equation governing the evolution of the probability to find a particle at position  $\mathbf{r}$ , going in direction  $\mathbf{u}$  reads

$$\partial_t P(\mathbf{r}, \mathbf{u}, t) = -\nabla \cdot [v(\mathbf{r})\mathbf{u}P(\mathbf{r}, \mathbf{u}, t)] + \Theta P(\mathbf{r}, \mathbf{u}, t) \quad (1.2)$$

where  $\Theta$  is a linear operator accounting for the dynamics of  $\mathbf{u}$ . In 2D, the particle orientation can be parametrized as  $\mathbf{u} = (\cos \theta, \sin \theta)$ . ABPs then correspond to  $\Theta P(\mathbf{r}, \theta) = D_r \partial_{\theta\theta} P(\mathbf{r}, \theta)$ , while RTPs are described by  $\Theta P = -\alpha P(\mathbf{r}, \theta) + \int \frac{\alpha d\theta'}{2\pi} P(\mathbf{r}, \theta')$ . In both cases, the steady-state solution of (1.2) simply reads

$$P(\mathbf{r}, \mathbf{u}) = \kappa/v(\mathbf{r}), \quad (1.3)$$

where  $\kappa$  is a constant ensuring normalization. Active particles thus accumulate where they move slower, with the  $1/v(\mathbf{r})$  scaling simply measuring the variation in residence time when the propulsion speed is non-uniform. It is interesting to note that gradients of  $v(\mathbf{r})$ , which locally break the isotropy of space, do not lead to a locally anisotropic distribution of orientations.

This simple result has been verified experimentally and used to control the spatial organisation of bacteria. Using bacteria whose swim speed can be controlled by light, the spatial modulation of the light field can be used to generate a position-dependent  $v(\mathbf{r})$ . In turn, this allows organizing the bacteria into complex patterns,<sup>22,23</sup> as shown in Fig.1.4.

The instability leading to MIPS then emerges from the interplay between this tendency of active particles to accumulate where they go slower and interactions that slow down the particles at high density. The particles then tend to accumulate where they are already atypically dense,



Figure 1.4: Experiments on light-activated bacteria where Eq. (1.3) is used to control the spatial organization of the bacteria. (a) The bacteria converge into a smiley pattern. (b) Pattern in bacterial density created after illuminating the bacteria with the light pattern shown in (c). Panel (a) is reproduced from Ref.<sup>22</sup> and panels (b,c) from Ref.<sup>23</sup> All are under the Creative Commons licence.

hence triggering phase separation. Interestingly, this narrative can be turned into a quantitative criterion to predict a linear instability.

Consider QSAPs that move at a speed locally given by  $v(\rho(\mathbf{r}))$ . Let us study the fate of a small fluctuation of the density field,  $\rho(\mathbf{r}) = \rho_0 + \delta\rho(\mathbf{r})$ , around its average value  $\rho_0$  (See Fig. 1.5). To linear order, the velocity is given by

$$v(\rho(\mathbf{r})) = v(\rho_0) + \delta\rho(\mathbf{r})v'(\rho_0) \quad (1.4)$$

where  $v'(\rho_0) \equiv dv/d\rho$  at  $\rho = \rho_0$ . As we have shown above, the density field tends to relax toward  $\rho(\mathbf{r}) = \tilde{\kappa}/v(\rho(\mathbf{r}))$  where  $\tilde{\kappa}$  is a normalization constant. Using Eq. (1.4), one finds, to first order in  $\delta\rho$ ,

$$\rho(\mathbf{r}) = \frac{\tilde{\kappa}}{v(\rho_0)} \left( 1 - \frac{v'(\rho_0)\delta\rho}{v(\rho_0)} \right). \quad (1.5)$$

Mass conservation imposes  $\int d\mathbf{r}\delta\rho(\mathbf{r}) = 0$  so that integrating Eq. (1.5) over space leads to  $\tilde{\kappa} = \rho_0 v(\rho_0)$ . The density field then tends to relax towards a new perturbation  $\rho(\mathbf{r}) \equiv \rho_0 + \delta\tilde{\rho}$ , with

$$\delta\tilde{\rho} = -\rho_0 \frac{v'(\rho_0)}{v(\rho_0)} \delta\rho \quad (1.6)$$

This means that the initial perturbation is amplified whenever the decrease of  $v$  with  $\rho_0$  is sufficiently strong:

$$\frac{v'(\rho_0)}{v(\rho_0)} < -\frac{1}{\rho_0} \quad \text{i.e.} \quad \frac{d}{d\rho_0}[\rho_0 v(\rho_0)] < 0. \quad (1.7)$$

The instability criterion (1.7) will be derived more rigorously in Section 1.6. However, this heuristic argument already captures qualitatively the instability mechanism leading to MIPS in most models. Although it is derived for QSAPs moving with a speed  $v(\rho(\mathbf{r}))$ , it applies also to  $N$  PFAPs for which an effective propulsion speed can be defined as  $v_{\text{eff}} \equiv N^{-1} \sum_i \langle \dot{\mathbf{r}}_i \cdot \mathbf{u}_i \rangle$ . This effective speed, which is averaged over all the particles, measures how fast particles move along their orientations. It tends to decrease with increasing density because of collisions. Simulation measurements show a linear decay  $v_{\text{eff}}(\rho_0) = v_0 - c\rho_0$ , with a constant  $c$ , up to rather high packing fractions,<sup>24</sup> which indeed satisfy the instability criterion Eq. (1.7) as soon as  $\rho_0 > 1/(2c)$ .

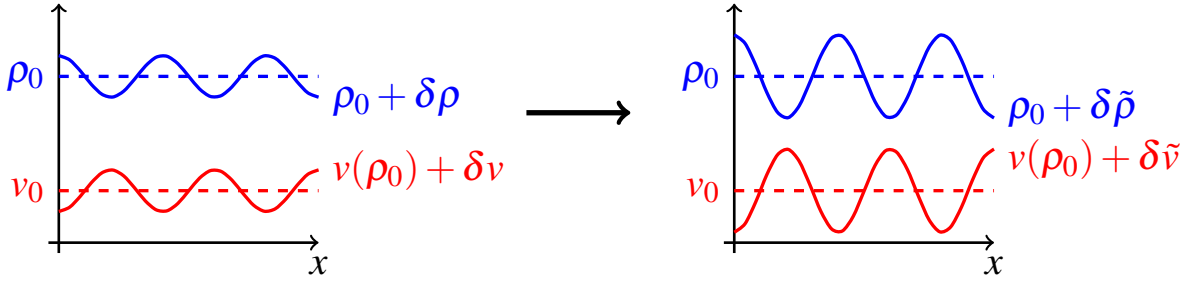


Figure 1.5: Illustration of the linear instability leading to MIPS. An initial density fluctuation leads to a modulation in propulsion speed. If  $v(\rho_0)$  decreases sufficiently fast with the density  $\rho_0$ , satisfying the criterion Eq. (1.7), it leads in turn to amplifying the density fluctuation. The homogeneous system is then linearly unstable.

## 1.4 Large-scale long-time description in the presence of position-dependent propulsion speed

Before discussing in more details the case of interacting particles, let us consider the long-time large-scale dynamics of  $N$  non-interacting active particles with a position-dependent self-propulsion speed  $v(\mathbf{r})$  that varies slowly in space: in a system of size  $L$ , we consider  $|\nabla v| \sim \mathcal{O}(L^{-1})$ .

### 1.4.1 A Fokker-Planck approximation

For the sake of clarity, we start from the case of a single particle, work in two space dimensions, and consider only tumbles with rate  $\alpha$ . The generalization to rotational diffusion and higher dimensions is straightforward.<sup>25</sup> We also account for the presence of Brownian noise leading to a translational diffusivity  $D_t$ . The master equation describing the dynamics is then given by

$$\partial_t P(\mathbf{r}, \theta, t) = -\nabla \cdot [v(\mathbf{r})\mathbf{u}(\theta)P(\mathbf{r}, \theta, t) - D_t \nabla P(\mathbf{r}, \theta, t)] - \alpha P(\mathbf{r}, \theta, t) + \frac{\alpha}{2\pi} p(\mathbf{r}, t) \quad (1.8)$$

where we have introduced the probability density to find the particle at position  $\mathbf{r}$ , irrespective of its direction,

$$p(\mathbf{r}, t) = \int d\theta P(\mathbf{r}, \theta, t) \quad (1.9)$$

Let us now construct the long-time large-scale dynamics of  $p(\mathbf{r}, t)$ . Integrating Eq. (1.8) over  $\theta$  leads to

$$\partial_t p(\mathbf{r}, t) = -\nabla \cdot [v(\mathbf{r})\mathbf{m}(\mathbf{r}, t)] + D_t \nabla^2 p(\mathbf{r}, t) \quad \text{where} \quad \mathbf{m}(\mathbf{r}, t) \equiv \int d\theta \mathbf{u}(\theta) P(\mathbf{r}, \theta, t). \quad (1.10)$$

The field  $\mathbf{m}(\mathbf{r}, t)$  measures the average orientation of the particle at position  $\mathbf{r}$ , whereas  $v(\mathbf{r})\mathbf{m}(\mathbf{r}, t)$  is the contribution to the current in position space due to self-propulsion. To close the dynamics of  $p(\mathbf{r}, t)$ , it is useful to compute that of  $\mathbf{m}(\mathbf{r}, t)$  by multiplying Eq. (1.8) by  $\mathbf{u}(\theta)$  and integrating over  $\theta$ . Component per component, this leads to

$$\partial_t m_i(\mathbf{r}, t) = -\partial_j \cdot \left[ v(\mathbf{r}) \int d\theta u_i u_j P(\mathbf{r}, \theta, t) \right] + D_t \nabla^2 m_i(\mathbf{r}, t) - \alpha m_i(\mathbf{r}, t), \quad (1.11)$$

where  $\partial_j \equiv \frac{\partial}{\partial x_j}$  is a short-hand notation for the  $j^{\text{th}}$  component of the gradient operator. In all the Chapter, summation over repeated indices is implied. Introducing the tensor  $Q_{ij}(\mathbf{r}) = \int d\theta [u_i u_j - \frac{\delta_{ij}}{2}] P(\mathbf{r}, \theta)$ , which measures the average local nematic order, the dynamics of  $\mathbf{m}(\mathbf{r}, t)$  can then be written as

$$\partial_t \mathbf{m}(\mathbf{r}, t) = -\nabla \left[ \frac{v(\mathbf{r})}{2} p \right] - \nabla \cdot [v(\mathbf{r}) \mathbf{Q}(\mathbf{r})] + D_t \nabla^2 \mathbf{m}(\mathbf{r}, t) - \alpha \mathbf{m}(\mathbf{r}, t). \quad (1.12)$$

Finally, multiplying Eq. (1.8) by  $u_i u_j - \frac{\delta_{ij}}{2}$  and integrating over  $\theta$  shows the dynamics of  $Q_{ij}$  to take the form

$$\partial_t Q_{ij}(\mathbf{r}, t) = -\nabla \cdot [\dots] - \alpha Q_{ij}(\mathbf{r}, t), \quad (1.13)$$

where the precise form of the gradient term will be shown to be irrelevant. The Equations (1.10), (1.12) and (1.13) are the three first equations of an infinite hierarchy that couples the dynamics of the various moments of  $P(\mathbf{r}, \theta)$ . Let us now show that, in the long-time large-scale limit, we can close this hierarchy.

In the presence of a field  $v(\mathbf{r})$  varying smoothly over a large scale  $L$ , the steady-state solution in the absence of translational diffusivity satisfies  $P(\mathbf{r}, \theta) \propto 1/v(\mathbf{r})$ , and it thus reproduces the smooth large-scale variations of  $v(\mathbf{r})$  as long as the latter remain bounded away from zero. The Brownian noise is only expected to alter quantitatively this behaviour and we thus expect the late-time dynamics of  $p(\mathbf{r})$  to describe the relaxation of large wave-length modes. Since  $p(\mathbf{r})$  is a conserved field, the time it takes to relax over a length scale  $L$  diverges as  $L \rightarrow \infty$ :  $p(\mathbf{r})$  is a slow, hydrodynamic mode. On the contrary, the dynamics (1.12) and (1.13) show the relaxation times of  $\mathbf{m}(\mathbf{r})$  and  $\mathbf{Q}(\mathbf{r})$  to scale as  $\alpha^{-1}$ , which remains finite as  $L$  diverges. These fast modes are thus enslaved to the sole slow mode  $p(\mathbf{r}, t)$ :  $\mathbf{m}(\mathbf{r}, t)$  and  $Q_{ij}(\mathbf{r}, t)$  follow quasi-statically the solutions of Eq. (1.12) and (1.13) in which we set  $\partial_t \mathbf{m} = \partial_t Q_{ij} = 0$ . Furthermore, in the limit of large  $L$ ,  $|\nabla v| \sim \mathcal{O}(L^{-1})$  so that all the fields are expected to vary slowly in space and, as we now show, we can use a gradient expansion to close the dynamics for  $p(\mathbf{r})$ . Inspection of Eq. (1.13) shows that, to leading order,  $Q_{ij} \sim \mathcal{O}(\nabla) \sim \mathcal{O}(L^{-1})$ . In turns, this leads to

$$\mathbf{m}(\mathbf{r}, t) \simeq -\frac{1}{\alpha} \nabla \left[ \frac{v(\mathbf{r})}{2} p(\mathbf{r}) \right] + \mathcal{O}(\nabla^2) \quad (1.14)$$

Inserting Eq. (1.14) into Eq. (1.10) then leads, to leading order, to the following dynamics for  $p(\mathbf{r})$ :

$$\partial_t p(\mathbf{r}, t) = \nabla \cdot \left[ \frac{v(\mathbf{r})}{2\alpha} \nabla [v(\mathbf{r}) p(\mathbf{r}, t)] + D_t \nabla p(\mathbf{r}, t) \right]. \quad (1.15)$$

A first interesting result that can be obtained from Eq. (1.15) is that the flux-free steady-state distribution satisfies

$$\frac{v(\mathbf{r}) \nabla [v(\mathbf{r})]}{2\alpha} p(\mathbf{r}, t) = - \left( \frac{v^2(\mathbf{r})}{2\alpha} + D_t \right) \nabla p(\mathbf{r}) \quad \text{so that} \quad \nabla \ln p(\mathbf{r}) = -\frac{1}{2} \nabla \ln \left( \frac{v^2(\mathbf{r})}{2\alpha} + D_t \right) \quad (1.16)$$

To leading order in gradients, the steady-state distribution is thus given by

$$p(\mathbf{r}) \propto \frac{1}{\sqrt{\frac{v^2(\mathbf{r})}{2\alpha} + D_t}}, \quad (1.17)$$

where, again, we disregard normalization issues. This result generalizes Eq. (1.3) to finite translational diffusion in the presence of smooth large-scale variations of  $v(\mathbf{r})$ . Introducing  $D_0 = v^2/(2\alpha)$ , which is the large-scale effective diffusivity of an RTP of self-propulsion speed  $v$  in 2d, the steady-state distribution  $p(\mathbf{r})$  is then found to be, to first order in  $D_t$ ,  $p \propto v^{-1}(1 - \frac{D_t}{2D_0})$ . As expected,  $D_t$  can be neglected when it is much smaller than  $D_0$ .

Reproducing the computations above in  $d$  space dimensions and including rotational diffusion as well as tumbles leads to a late-time dynamics:<sup>25</sup>

$$\partial_t p(\mathbf{r}, t) = \nabla \cdot [\nabla [D_c(\mathbf{r})p(\mathbf{r}, t)] - \mathbf{F}(\mathbf{r})p(\mathbf{r}, t)] \quad (1.18)$$

where

$$D_c(\mathbf{r}) = D_t + \frac{v^2(\mathbf{r})\tau}{d} \quad \text{and} \quad \mathbf{F}(\mathbf{r}) = \frac{1}{2}\nabla \left[ D_t + \frac{v^2(\mathbf{r})\tau}{d} \right] \quad (1.19)$$

and we have introduced the persistence time of the active particle

$$\tau \equiv [\alpha + (d-1)D_r]^{-1}. \quad (1.20)$$

The dynamics (1.18) is nothing but a Fokker-Planck approximation to the active dynamics in the presence of a non-uniform self-propulsion speed. Having integrated out the orientational degrees of freedom of the active particles, the long-time large-scale dynamics of their positions are thus equivalent to an Itô-Langevin dynamics:

$$\dot{\mathbf{r}} = \mathbf{F}(\mathbf{r}) + \sqrt{2D_c}\boldsymbol{\eta}, \quad (1.21)$$

where  $\boldsymbol{\eta}$  is a  $d$ -dimensional Gaussian white noise whose spatial components satisfy  $\langle \eta_\mu \eta_\nu \rangle = \delta_{\mu\nu} \delta(t - t')$ .

A number of comments are in order. First, the steady-state solution (1.17) is a flux-free solution of the Fokker-Planck equation (1.18). It thus corresponds to an equilibrium state: the microscopic, non-equilibrium nature of the active dynamics has disappeared upon coarse-graining. Then, inspection of the Itô-Langevin dynamics (1.21) shows that  $\mathbf{F}$  and  $\sqrt{2D_c}\boldsymbol{\eta}_i$  favors opposite trends for the particles:  $\mathbf{F}$  drives particles towards high-speed regions whereas  $\sqrt{2D_c}\boldsymbol{\eta}_i$  drives them towards low-activity ones. Finally, note that Eq. (1.18) also corresponds to a Stratonovich-Langevin dynamics, which would also be given by Eq. (1.21), albeit with  $\mathbf{F} = 0$ . In the next section, we will use Itô calculus to construct the fluctuating hydrodynamics describing  $N$  non-interacting active particles and we will thus stick to the Itô prescription.

## 1.4.2 Fluctuating hydrodynamics

To keep notations as light as possible, we first work in one dimension before generalizing our results to higher dimensions. We consider  $N$  active particles at positions  $x_i$ , evolving in a field  $v(x)$ , in the limit in which the particle dynamics are well approximated by Eq. (1.21). The purpose of this section is to describe the stochastic evolution of the density field

$$\hat{\rho}(x, t) = \sum_{i=1}^N \delta[x - x_i(t)]. \quad (1.22)$$

Note that the time dependency of  $\hat{\rho}(x, t)$  solely stems from that of  $x_i(t)$ . Constructing the dynamics of the density field thus amounts to applying the chain rule to Eq. (1.22). This is,

however, a non-trivial task because  $x_i(t)$  is far from being a smooth function of time. The standard chain rule, built using differential calculus, fails for stochastic dynamics like Eq. (1.21). Instead, a proper regularization is needed, using stochastic calculus, which leads to the so-called Itô-formula. A rigorous derivation of the latter can be found in textbooks on stochastic calculus<sup>26</sup> and we instead present here a heuristic approach.

To determine  $\frac{d}{dt}\hat{\rho}(x,t)$ , we need to estimate  $\Delta\rho_i(t) \equiv \delta[x - x_i(t + dt)] - \delta[x - x_i(t)]$  to first order in  $dt$ . Taylor-expanding  $\Delta\rho_i$  to second order yields

$$\frac{\Delta\rho_i(t)}{dt} = -\frac{x_i(t + dt) - x_i(t)}{dt} \frac{\partial}{\partial x} \delta[x - x_i(t)] + \frac{1}{2} \frac{[x_i(t + dt) - x_i(t)]^2}{dt} \frac{\partial^2}{\partial x^2} \delta[x - x_i(t)]. \quad (1.23)$$

The first term on the right-hand side yields  $-\dot{x}_i\delta'[x - x_i(t)]$  when  $dt$  is sent to zero. In the usual chain rule, this is the sole contribution to  $\partial_t\delta[x - x_i(t)]$  and the second term in the right-hand side of Eq. (1.23) can be neglected. Let us now show that this is not the case here. To leading order in  $dt$ , integrating Eq. (1.21) in 1d between  $t$  and  $t + dt$  leads to

$$\begin{aligned} \Delta x_i(t) \equiv x_i(t + dt) - x_i(t) &= \int_t^{t+dt} ds F[x_i(s)] + \int_t^{t+dt} ds \sqrt{2D_c[x_i(s)]} \eta_i(s) \\ &\simeq F[x_i(t)]dt + \sqrt{2D_c[x_i(t)]} d\eta_i(t), \end{aligned} \quad (1.24)$$

where we have introduced  $d\eta_i(t) \equiv \int_t^{t+dt} ds \eta_i(s)$ . Taking the square of Eq.(1.24) then leads to  $\Delta x_i(t)^2 = 2D_c[x_i(t)]d\eta_i(t)^2 + o(dt)$ , where we have used that  $d\eta_i(t)$  vanishes as  $dt$  goes to zero. The second term in the right-hand side of Eq. (1.23) will thus contribute if  $d\eta_i(t)^2$  is of order  $dt$ . To show that this is indeed the case, we compute the successive moments of  $d\eta_i(t)^2$ :

$$\langle d\eta_i(t)^2 \rangle = \int_t^{t+dt} du \int_t^{t+dt} ds \langle \eta_i(s) \eta_i(u) \rangle = \int_t^{t+dt} du \int_t^{t+dt} ds \delta(s - u) = dt$$

The average of the random variable  $d\eta_i(t)^2$  is thus equal to  $dt$ . The higher moments of  $d\eta_i(t)^2$ , which characterize its fluctuations, can be computed using Wick theorem; they are negligible to order  $dt$ . For instance,  $\langle d\eta_i(t)^4 \rangle = 6D_c[x_i(t)]^2 dt^2$ . It is thus tempting to simply replace  $[x_i(t + dt) - x_i(t)]^2$  by its average value  $2D_c[x_i(t)]dt$  in Eq. (1.23). This would lead to:

$$\partial_t \delta[x - x_i(t)] = -\dot{x}_i(t) \partial_x \delta[x - x_i(t)] + D[x_i(t)] \partial_{xx} \delta[x - x_i(t)], \quad (1.25)$$

which is indeed the result of applying Itô formula to  $\delta[x - x_i(t)]$ . Note that a rigorous construction of Itô formula is significantly more involved than the hand-waving argument above and it involves clarifying the meaning of the equality in (1.25).<sup>26</sup>

Using that, for all functions  $f$ ,

$$f(x_i) \partial_x \delta(x - x_i) = \partial_x [f(x_i) \delta(x - x_i)] = \partial_x [f(x) \delta(x - x_i)], \quad (1.26)$$

Eq. (1.25) can be rewritten as

$$\partial_t \delta[x - x_i(t)] = -\partial_x \left[ F(x) \delta[x - x_i(t)] + \sqrt{2D[x(t)]} \eta_i \delta(x - x_i) - \partial_x [D[x(t)] \delta[x - x_i(t)]] \right] \quad (1.27)$$

Summing upon  $i$  then leads to

$$\partial_t \rho(x,t) = -\partial_x \left[ F(x) \rho(x,t) + \sqrt{2D[x(t)]} \Lambda(x,t) - \partial_x [D[x(t)] \rho(x,t)] \right], \quad (1.28)$$

where  $\Lambda(x, t)$  is a Gaussian noise field of zero mean and unit variance and we used that:<sup>27</sup>

$$\left\langle \sum_{i,j} \delta[x - x_i(t)] \eta_i(t) \delta[x' - x_j(t')] \eta_j(t') \right\rangle = \rho(x, t) \delta(t - t') \delta(x - x'). \quad (1.29)$$

The above derivation can be reproduced in higher dimensions. Using the expressions (1.19) for  $D_c$  and  $F$ , it leads to

$$\partial_t \rho(\mathbf{r}, t) = \nabla \cdot \left[ M \nabla \mu(\mathbf{r}, [\rho]) + \sqrt{2M} \Lambda(\mathbf{r}, t) \right] \quad (1.30)$$

where  $\mu$  acts as a chemical potential given by

$$\mu(\mathbf{r}, [\rho]) = \ln \left[ \rho(\mathbf{r}) \sqrt{D_c(\mathbf{r})} \right] \quad (1.31)$$

and the collective mobility  $M$  reads

$$M(\mathbf{r}) = \rho(\mathbf{r}) D_c(\mathbf{r}) \quad \text{with} \quad D_c(\mathbf{r}) = D_t + \frac{v^2(\mathbf{r}) \tau}{d}. \quad (1.32)$$

Equation (1.21) is a diffusive approximation, at the single-particle level, of a run-and-tumble dynamics with position-dependent self-propulsion speed  $v(\mathbf{r})$ . In Section 1.4.1, we have shown that this approximate dynamics satisfies detailed balance and thus amounts to an equilibrium dynamics. Equations (1.30), (1.31) and (1.32) are its collective counterparts. Naturally, they also correspond to an equilibrium dynamics and the chemical potential  $\mu$  is the functional derivative of a free energy:

$$\mu(\mathbf{r}, [\rho]) = \frac{\delta \mathcal{F}[\rho]}{\delta \rho(\mathbf{r})} \quad \text{with} \quad \mathcal{F}[\rho] = \int d\mathbf{r} \left[ \rho(\mathbf{r}) [\ln \rho(\mathbf{r}) - 1] + \frac{1}{2} \rho(\mathbf{r}) \ln [D_c(\mathbf{r})] \right] \quad (1.33)$$

The first term in the effective free energy  $\mathcal{F}$  is an entropic term, which conveys that the persistent random walks of run-and-tumble particles favor a uniform spreading of the particles in space. The second term stems from the tendency of active particles to accumulate where they go slower. Here, this takes the form of an effective potential energy  $U(\mathbf{r}) = \ln[D_c(\mathbf{r})]/2$ . Equation (1.33) thus reveals an intriguing mapping between active particles whose self-propulsion is non-uniform and passive particles in potential energy landscapes. As we shall show in the next section, this analogy partially extends to interacting dynamics.

## 1.5 Fluctuating hydrodynamics of Active Particles interacting via Quorum-Sensing (QSAPs)

Quorum-sensing interactions are common in the biological world where they describe situations in which the behaviours of individuals are affected by the local density of their surrounding peers. A pedestrian adapting its walking speed depending on the density of the surrounding crowd is a simple macroscopic example of such interactions. At the microscopic scale, quorum-sensing interactions are frequent among cells, where they are typically mediated by signaling molecules. In a bacterial population, a common mechanism is the production of auto-inducers,

like acylated homoserine lactones, which then diffuse in the surrounding medium and regulate the gene expressions of other bacteria. In this section, we retain this framework to make contact with recent experiments on bacterial colonies in which the cell motility is regulated by quorum-sensing.<sup>17,28</sup> To lighten the notation, we neglect  $D_t$ , which is typically three orders of magnitudes smaller than  $D_0$  for swimming *E. coli*.<sup>29,30</sup>

We note  $c(\mathbf{r})$  the concentration field of signaling molecules produced by the bacteria at rate  $\beta$ . After their production, these molecules diffuse in the surrounding medium with a diffusivity  $D$  and they are degraded with a rate  $\gamma$ , leading to the dynamics

$$\dot{c}(\mathbf{r}, t) = D\Delta c(\mathbf{r}, t) - \gamma c(\mathbf{r}, t) + \beta \rho(\mathbf{r}, t) \quad (1.34)$$

We aim at describing the large-scale collective dynamics of our bacterial assembly on time scales where the division and death of bacteria can be neglected, so that the bacterial density field satisfies a conservation law  $\partial_t \rho(\mathbf{r}, t) = -\nabla \cdot \mathbf{J}(\mathbf{r}, [\rho])$ , where ‘ $[\rho]$ ’ refers to a functional dependence of the current  $\mathbf{J}$  on the density field  $\rho(\mathbf{r}, t)$ . The relaxation of a density modulation  $\delta\rho(x)$  around a homogeneous profile  $\rho_0$  then satisfies

$$\partial_t \delta\rho(\mathbf{r}, t) = -\nabla \cdot \int d\mathbf{r}' \frac{\delta\mathbf{J}(\mathbf{r}, [\rho_0])}{\delta\rho(\mathbf{r}')} \delta\rho(\mathbf{r}', t). \quad (1.35)$$

When the system is invariant under translation,  $\frac{\delta\mathbf{J}(\mathbf{r}, [\rho_0])}{\delta\rho(\mathbf{r}')} \equiv \mathbf{K}(\mathbf{r} - \mathbf{r}', \rho_0)$  only depends on  $\mathbf{r} - \mathbf{r}'$  so that, in Fourier space, the dynamics of the Fourier modes decouple:

$$\partial_t \delta\rho(\mathbf{q}, t) = i\mathbf{q} \cdot \mathbf{K}(\mathbf{q}, \rho_0) \delta\rho(\mathbf{q}, t). \quad (1.36)$$

The typical relaxation time of the Fourier mode  $\delta\rho(\mathbf{q}, t)$  thus diverges as  $[\mathbf{q} \cdot \mathbf{K}(\mathbf{q}, \rho_0)]^{-1}$  as  $q \rightarrow 0$ : large-scale modes take a macroscopic time to relax since matter has to be transported over a macroscopic size, which necessarily takes a macroscopic time at finite speed. Equation (1.36) is the generic reason why a hydrodynamic field can be associated to any conservation law. Here, mass conservation makes the density field a slow field.

On the contrary, the dynamics (1.34) leads to a finite relaxation time  $\tau_q \sim \gamma^{-1}$  as  $q \rightarrow 0$  and we can thus consider that  $c(\mathbf{r}, t)$  follows adiabatically the solution of

$$(\gamma - D\Delta)c(\mathbf{r}, t) = \beta\rho(\mathbf{r}, t) \quad (1.37)$$

which is nothing but a screened Poisson dynamics for the field  $c(\mathbf{r}, t)$  in the presence of a source field proportional to  $\rho(\mathbf{r}, t)$ . Equation (1.37) can be solved as

$$c(\mathbf{r}, t) = \int d\mathbf{r}' G(\mathbf{r} - \mathbf{r}') \rho(\mathbf{r}', t), \quad (1.38)$$

where  $G$  is the corresponding Green’s function,<sup>31</sup> which satisfies

$$\left( \frac{\gamma}{\beta} - \frac{D}{\beta} \Delta \right) G(\mathbf{r}) = \delta(\mathbf{r}). \quad (1.39)$$

The concentration of signaling molecules thus acts as a slightly non-local proxy for the bacterial concentration through Eq. (1.38).

In turn, bacteria adapt their swimming patterns to the local concentration  $c(\mathbf{r}, t)$ . Once the concentration field has been eliminated using Eq. (1.38), the microscopic parameters of the run-and-tumble dynamics, like the swim speed  $v$  or the tumbling rate  $\alpha$ , thus depend on  $\rho$  in a slightly non-local way. Note that quorum-sensing in bacterial suspensions involves a delay between the variation of the level of a signaling molecules  $c(\mathbf{r}, t)$  and the change of the expression level of the proteins under the control of the auto-inducer. In turn, this implies a delay between the variation of  $c(\mathbf{r}, t)$  and the adaptation of the swimming pattern of the bacteria. We neglect this aspect here, assuming again that  $c(\mathbf{r}, t)$  evolves slowly, following  $\rho(\mathbf{r}, t)$  adiabatically. The coarse-grained dynamics of run-and-tumble bacteria whose tumbling rate, duration and swimming speed depend on the local density can be computed using the methods described in this chapter.<sup>25,28,32</sup> For simplicity, we discuss here only the case in which the velocity is influenced by the local density.

Finally, the approximation of the run-and-tumble dynamics by a diffusive one takes place on a time scale that is large compared to the tumbling rates and durations, but which is small compared to that governing the large-scale dynamics of the density field. We can thus treat a self-propulsion speed  $v(\mathbf{r}, [\rho])$  as simply depending on  $\mathbf{r}$  to coarse-grain the bacterial dynamics into its diffusion-drift approximation (1.21) and only let  $\rho(\mathbf{r}, t)$  evolve on much larger time scales. The result of this adiabatic treatment is to predict an evolution of the density field given by

$$\partial_t \rho(\mathbf{r}, t) = \nabla \cdot [M \nabla \mu(\mathbf{r}, [\rho])] + \sqrt{2M} \Lambda(\mathbf{r}, t) \quad (1.40)$$

where  $\mu$  and  $M$  are now given by

$$\mu(\mathbf{r}, [\rho]) = \ln[\rho(\mathbf{r})v(\mathbf{r}, [\rho])] \quad \text{and} \quad M = \rho(\mathbf{r}) \frac{v^2(\mathbf{r}, [\rho])\tau}{d}. \quad (1.41)$$

Note that going from the Langevin dynamics (1.21) to the stochastic field dynamics (1.40) when the velocity is a functional of the density field is actually trickier than what was presented in Section 1.4.2 because of the non-local dependency of  $M$  on the field  $\rho$ . The corresponding multiplicative noise has to be handled with care and, in practice, Eq. (1.40) is valid for kernels  $G$  which are symmetric.<sup>32</sup>

We now turn to the analysis of the dynamics (1.40) to characterize the motility-induced phase separation that can emerge from quorum-sensing interactions.

## 1.6 Generalized thermodynamics of QSAPs

In general, the stochastic field theory (1.40) does not describe an equilibrium dynamics and its steady-state distribution  $P[\rho]$  is unknown. However, we show in this section that there are a number of cases in which connection with equilibrium physics can be made.

Let us first note that the noise amplitude and the mobility are both given by  $M(\mathbf{r}, [\rho])$  and thus satisfy a Stokes-Einstein relation. At this level of description, it is thus not the noise entering the field theory that drives the system out of equilibrium.

The same cannot be said, however, for the generalized chemical potential  $\mu(\mathbf{r}, [\rho])$ . The latter induces an equilibrium dynamics if and only if it can be written as the functional derivative

of a free energy, *i.e.* iff there is a functional  $\mathcal{F}[\rho]$  such that

$$\mu(\mathbf{r}, [\rho]) = \frac{\delta \mathcal{F}[\rho]}{\delta \rho(\mathbf{r})}. \quad (1.42)$$

Equation (1.42) need not admit a solution for arbitrary functionals  $\mu(\mathbf{r}, [\rho])$ . In finite dimensions, the Poincare lemma tells us that a vector field  $\mathbf{F}$  is a gradient if its cross derivatives are equal<sup>1</sup>:  $\partial_i F_j = \partial_j F_i$ . This can be generalized to our field theory and Eq. (1.42) admits a solution if and only if:<sup>33</sup>

$$\mathcal{D}(\mathbf{r}, \mathbf{r}') = \frac{\delta \mu(\mathbf{r}, [\rho])}{\delta \rho(\mathbf{r}')} - \frac{\delta \mu(\mathbf{r}', [\rho])}{\delta \rho(\mathbf{r})} = 0. \quad (1.43)$$

Note that Eq. (1.43) has to be understood in the sense of distributions, *i.e.* for any functions  $\phi(\mathbf{r})$ ,  $\psi(\mathbf{r}')$ , one needs  $\int d\mathbf{r} d\mathbf{r}' \mathcal{D}(\mathbf{r}, \mathbf{r}') \phi(\mathbf{r}) \psi(\mathbf{r}') = 0$ .

Consider, as an example, the case of  $\mu(x, [\rho]) = \partial_x^k \rho(x)$  in one dimension. Then,  $\mathcal{D}(x, x') = (\partial_x^k - \partial_{x'}^k) \delta(x - x')$  and the integrability condition (1.43) reads

$$0 = \int dx [\phi^{(k)}(x) \psi(x) - \phi(x) \psi^{(k)}(x)] = \int dx \phi^{(k)}(x) \psi(x) [1 - (-1)^k] \quad (1.44)$$

where the second equality stems from integrating by parts  $k$  times. This condition holds for any pair of functions  $(\psi, \phi)$  if and only if  $k$  is an even number. In this case, the free energy is given by  $\mathcal{F} = \frac{1}{2} \int dx (-1)^n (\partial_x^n \rho)^2$ , where  $n = k/2$ . Let us now study the conditions under which the large-scale dynamics of run-and-tumble particles interacting via quorum sensing admit a coarse-grained equilibrium description.

### 1.6.1 The local approximation: an equilibrium theory

The self-propulsion speed  $v(\mathbf{r}, [\rho])$  depends on the density through the concentration  $c(\mathbf{r}, t)$  and can thus be written as

$$v(\mathbf{r}, [\rho]) = v[\tilde{\rho}(\mathbf{r})] \quad \text{with} \quad \tilde{\rho}(\mathbf{r}) = \int d\mathbf{r}' G(\mathbf{r} - \mathbf{r}') \rho(\mathbf{r}'). \quad (1.45)$$

In Eq. (1.45), we have absorbed the normalization of  $G$  in the definition of the function  $v$  and set  $\int d\mathbf{r} G(\mathbf{r}) = 1$ , which amounts to multiplying the left-hand side of Eq. (1.39) by  $\beta/\gamma$ .  $\tilde{\rho}(\mathbf{r})$  is then the coarse-grained density measured at position  $\mathbf{r}$  by the particles. Note that, because the diffusion of  $c$  is isotropic, so is  $G$ , leading to  $\int d\mathbf{r} \mathbf{r} G(\mathbf{r}) = 0$  and  $\int d\mathbf{r} r_i r_j G(\mathbf{r}) = \delta_{i,j} \ell_g^2$ . Using Eq. (1.39), one finds—up to the normalization mentioned above—that  $\ell_g = \sqrt{2D/\gamma}$ . The latter is the typical length over which the coarse-graining kernel  $G$  samples the density field; it corresponds to the typical length travelled by signaling molecules before they are degraded. When the density field varies over much larger length scales, it is natural to approximate  $\tilde{\rho}(\mathbf{r})$  as

$$\tilde{\rho}(\mathbf{r}) \simeq \int d\mathbf{r}' G(\mathbf{r}') [\rho(\mathbf{r}) - \mathbf{r}' \cdot \nabla \rho(\mathbf{r}) + \frac{1}{2} \mathbf{r}' \cdot \mathbf{H}(\mathbf{r}) \mathbf{r}'], \quad (1.46)$$

where  $H_{ij} = \partial_{i,j}^2 \rho(\mathbf{r})$ . Using the symmetry properties of  $G$ , this reduces to

$$\tilde{\rho}(\mathbf{r}) \simeq \rho(\mathbf{r}) + \frac{1}{2} \ell_g^2 \Delta \rho(\mathbf{r}). \quad (1.47)$$

---

<sup>1</sup>provided the space is simply connected

To leading order,  $\tilde{\rho}(\mathbf{r}) = \rho(\mathbf{r})$  and  $\mu(r, [\rho])$  is a local function of  $\rho(\mathbf{r})$ . In this local approximation, the integrability of  $\mu(\mathbf{r}) = \ln[\rho(\mathbf{r})v(\rho(\mathbf{r}))]$  is easily established since:

$$\mathcal{D}(\mathbf{r}, \mathbf{r}') = \left( \frac{1}{\rho(\mathbf{r})} + \frac{v'(\rho(\mathbf{r}))}{v(\rho(\mathbf{r}))} \right) \delta(\mathbf{r} - \mathbf{r}') - \left( \frac{1}{\rho(\mathbf{r}')} + \frac{v'(\rho(\mathbf{r}'))}{v(\rho(\mathbf{r}'))} \right) \delta(\mathbf{r}' - \mathbf{r}) = 0, \quad (1.48)$$

where we have introduced  $v'(\rho) \equiv \frac{dv(\rho)}{d\rho}$ . The free energy  $\mathcal{F}$  is then given by

$$\mathcal{F}[\rho] = \int d\mathbf{r} f(\rho(\mathbf{r})), \quad (1.49)$$

where  $f(\rho)$  is the free energy density, given by

$$f(\rho) = \rho(\ln \rho - 1) + \int^\rho ds \ln v(s). \quad (1.50)$$

(Note that the integral is taken with respect to the argument of  $v(\rho)$ ). Some comments are in order. First, the addition of a linear term  $\mu_0 \rho$  to  $f(\rho)$  simply leads to the constant shift

$$\mathcal{F} \rightarrow \mathcal{F} + \mu_0 \int d\mathbf{r} \rho(\mathbf{r}) = \mathcal{F} + \mu_0 N, \quad (1.51)$$

where  $N$  is the total number of particles. Since the latter is conserved, this shift does not change the relative weights of different density profiles. This thus means that rescaling the velocity  $v(s) \rightarrow z_0 v(s)$ , which induces such a shift with  $\mu_0 = \ln z_0$ , should not change the steady-state distribution. Here, nothing competes with  $v(\rho(\mathbf{r}))$  to set a scale above which MIPS can be observed. It would not be the case if we had retained a finite translational diffusion  $D_t$ . Then, there would be a minimal self-propulsion speed above which MIPS can be observed.<sup>4</sup>

Let us now use the expressions (1.49) and (1.50) to characterize the possibility of phase separation. When  $\mu = \frac{\delta \mathcal{F}}{\delta \rho}$ , the functional Fokker-Planck equation associated to (1.40) admits a flux-free steady-state solution  $P[\rho] = Z^{-1} \exp(-\mathcal{F}[\rho])$ . The most likely profiles are thus those which minimize  $\mathcal{F}[\rho]$ . For a fixed averaged density  $\rho_0$ , one should compare the free energy of the homogeneous profile to that of a phase separated profile between a gas at some density  $\rho_1$  and a liquid at density  $\rho_2$ , each occupying a fraction  $\alpha$  and  $1 - \alpha$  of the system, with mass conservation imposing that  $\rho_0 = \alpha \rho_1 + (1 - \alpha) \rho_2$ . The uniform profile then has free energy  $\mathcal{V} f(\rho_0) = \mathcal{V} f(\alpha \rho_1 + (1 - \alpha) \rho_2)$ , with  $\mathcal{V}$  the volume of the system, while the phase-separated profile has free energy  $\mathcal{V} [\alpha f(\rho_1) + (1 - \alpha) f(\rho_2)]$ . Phase separation is thus statistically favored whenever

$$\alpha f(\rho_1) + (1 - \alpha) f(\rho_2) < f(\alpha \rho_1 + (1 - \alpha) \rho_2), \quad (1.52)$$

which requires the function  $f(\rho)$  to be non-convex. On the contrary, when  $f(\rho)$  is convex, the uniform profile is always statistically favored. The two situations are illustrated in Fig. 1.6a-b.

Equation (1.52) may be satisfied by many different pairs  $(\rho_1, \rho_2)$  and a natural question is then which of these will be statistically favoured. The answer comes from constructing the convex envelope  $f_c(\rho)$  of  $f(\rho)$ . Regions in which  $f(\rho_0) = f_c(\rho_0)$  correspond to uniform phases. On the contrary, the system is phase-separated when  $f(\rho) > f_c(\rho)$ . In such a region,  $f_c(\rho)$  is a linear function interpolating between two densities such that  $f(\rho_g) = f_c(\rho_g)$  and  $f(\rho_\ell) = f_c(\rho_\ell)$ . The favoured solution within the region is then a phase-separated state between  $\rho_g$  and

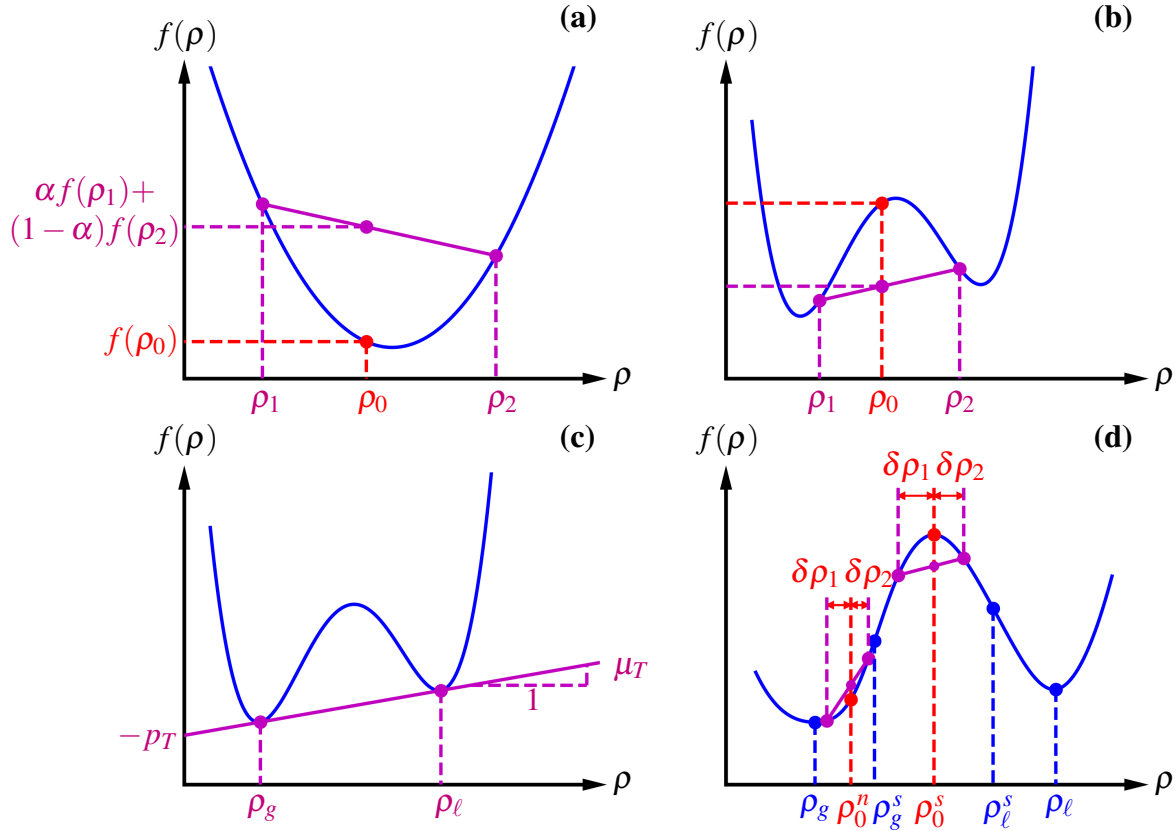


Figure 1.6: Analysis of phase separation based on the free-energy density  $f(\rho)$ . **(a)** When the free energy density is convex,  $f(\rho_0)$  is always lower than the free-energy density  $\alpha f(\rho_1) + (1 - \alpha)f(\rho_2)$  resulting from phase-separating between two densities  $\rho_1$  and  $\rho_2$  such that  $\alpha\rho_1 + (1 - \alpha)\rho_2 = \rho_0$ . **(b)** In a concave region of  $f(\rho)$ , the converse holds and phase separation is favored. **(c)** The most favorable phase-separated state involves  $\rho_g$  and  $\rho_\ell$ , which are the intersects between  $f(\rho)$  and the linear section of its convex envelope, and delimit the region where the two do not overlap. The magenta line is called the common tangent to  $f(\rho)$ , its slope corresponds to the thermodynamic chemical potential  $\mu_T$  while its intersect with the ordinate axis is given by the opposite of the thermodynamic pressure,  $p_T$ . **(d)** By comparing the free energy density of a uniform profile at density  $\rho_0$  and that of a coexistence state between densities  $\rho_0 - \delta\rho_1$  and  $\rho_0 + \delta\rho_2$ , one predicts that phase-separation is triggered by a linear instability whenever  $f''(\rho_0) < 0$ , whereas nucleation is required in  $[\rho_g, \rho_g^s] \cup [\rho_\ell^s, \rho_\ell]$ .

$\rho_\ell$ , where the relative fraction of each phase is set by the lever rule  $\rho_0 = \alpha\rho_g + (1 - \alpha)\rho_\ell$ . Geometrically, the liquid and gas densities are found by using the so-called common-tangent construction depicted in Fig. 1.6c.

Within the local approximation, we have thus established a direct mapping between our active system and a passive equilibrium, which allows discussing the existence of thermodynamic state variables. Indeed, the common-tangent construction, derived above from statistical arguments, also offers a thermodynamic interpretation. The fact that the slopes of  $f(\rho)$  are the same at  $\rho_g$  and  $\rho_\ell$  can be read as an equality of thermodynamic chemical potential, defined as  $\mu_T = \frac{\partial \mathcal{F}}{\partial N}$ , where  $N$  is the total number of particles. Using that  $\mathcal{F} \simeq \mathcal{V} f(\rho_0)$  and  $\rho_0 = N/\mathcal{V}$  indeed leads to  $\mu_T = \mathcal{V} f'(N/\mathcal{V})/\mathcal{V} = f'(\rho_0)$ , which allows identifying the value of field  $\mu(r, [\rho])$  in homogeneous phases with its thermodynamic counterpart in the macroscopic limit. Similarly, the thermodynamic pressure is defined as  $p_T = -\frac{\partial \mathcal{F}}{\partial \mathcal{V}} = -f(\rho_0) + \rho_0 f'(\rho_0)$ . The fact that the tangents to  $f(\rho)$  at  $\rho_g$  and  $\rho_\ell$  have the same intersect with the ordinate axis thus conveys the equality of thermodynamic pressure between the two phases.

The above discussion on the convexity of  $f(\rho_0)$  provides an intuitive understanding of the origin of phase separation and of the selection mechanism for the coexisting densities. For the sake of completeness, we mention that the mathematical derivation of the common-tangent construction is more easily obtained by minimizing the free energy constrained by the average density. To do so, consider the function

$$G(\alpha, \mu, \rho_g, \rho_\ell) = \alpha f(\rho_g) + (1 - \alpha)f(\rho_\ell) - \mu[\alpha\rho_g + (1 - \alpha)\rho_\ell - \rho_0], \quad (1.53)$$

where  $\mu$  plays the role of a Lagrange multiplier. Minimizing  $G$  with respect to  $\rho_g$  and  $\rho_\ell$  leads to the equality of chemical potentials,  $\mu = f'(\rho_g) = f'(\rho_\ell)$ . Then, minimizing  $G$  with respect to  $\alpha$  leads to the equality of pressures  $f(\rho_g) - \rho_g f'(\rho_g) = f(\rho_\ell) - \rho_\ell f'(\rho_\ell)$ . Minimizing  $G$  with respect to  $\mu$  finally imposes the lever rule  $\alpha = (\rho_0 - \rho_\ell)/(\rho_g - \rho_\ell)$ .

From  $f(\rho)$  we can thus predict whether the steady state of the system is phase separated. How then does the system dynamically reach the phase-separated state starting from an homogeneous one? A simple answer comes from looking at the role of small fluctuations: Would phase-separating between  $\rho_0 - \delta\rho_1$  and  $\rho_0 + \delta\rho_2$  lower the free energy? If so, then small fluctuations immediately trigger an instability ultimately leading to phase separation, which is indeed the case whenever  $f''(\rho_0) < 0$  *i.e.* when the free energy is locally concave. This phenomenon is termed spinodal decomposition and happens between the gas and liquid spinodals that we denote  $\rho_g^s$  and  $\rho_\ell^s$ . Using the explicit expression of  $f(\rho)$  given in Eq. (1.50), the spinodal region satisfies

$$\frac{1}{\rho_0} + \frac{v'(\rho_0)}{v(\rho_0)} < 0. \quad (1.54)$$

Interestingly, this is exactly the criterion (1.7) derived heuristically in Section 1.3. On the contrary in  $[\rho_g, \rho_g^s] \cup [\rho_\ell^s, \rho_\ell]$  the system is globally unstable but linear fluctuations will not suffice to lead to phase separation. In these region, nucleation is required to destabilize an initially homogeneous profile.

The local approximation is appealing because it offers a simple framework to predict the occurrence of motility-induced phase separation and captures quantitatively the linear instability criterion (1.54). However, it suffers from a major drawback: the measure corresponding to the free energy (1.49) is factorized and thus predicts all points in space to be statistically independent. There is thus no way to understand the physics of domain walls or coarsening within

this framework, nor to account for any spatial structure exhibited by the system. To fix this, a natural strategy is to go beyond the local approximation  $\tilde{\rho}(\mathbf{r}) = \rho(\mathbf{r})$ . This is the purpose of the next subsection which includes higher-order gradient terms. As we shall see, the mapping to equilibrium then breaks down and the connection to thermodynamics is lost. While the equality of ‘chemical potentials’ between coexisting phases is preserved, this is not true of  $p_T$ : because of gradient terms, the common-tangent construction will be replaced by an uncommon-tangent construction.<sup>34</sup>

## 1.6.2 Gradient expansion: beyond the local approximation

The next order expansion of  $v(r, [\rho])$  is obtained by using Eq. (1.47) to write  $\tilde{\rho} = \rho + \frac{D}{\gamma}\Delta\rho$ , which leads to a ‘quasi-local’ approximation

$$v(r, [\rho]) \simeq v(\rho(\mathbf{r})) + v'(\rho(\mathbf{r}))\frac{D}{\gamma}\Delta\rho(\mathbf{r}). \quad (1.55)$$

In turn, this leads to the generalized chemical potential

$$\mu(\mathbf{r}, [\rho]) = \ln[\rho(\mathbf{r})v(\rho(\mathbf{r}))] - \kappa(\rho(\mathbf{r}))\Delta\rho \quad \text{with} \quad \kappa(\rho(\mathbf{r})) = -\frac{Dv'(\rho(\mathbf{r}))}{\gamma v(\rho(\mathbf{r}))}. \quad (1.56)$$

### Equilibrium mapping

The local part of  $\mu$  in Eq. (1.56) is nothing but the local theory developed in the previous subsection. It can be integrated functionally to lead to the free energy density (1.50).

To check the conditions under which  $-\kappa(\rho)\Delta\rho$  is a functional derivative, we use Eq. (1.43) to compute its contribution to  $\mathcal{D}(\mathbf{r}, \mathbf{r}')$ , which leads to

$$\mathcal{D}(\mathbf{r}, \mathbf{r}') = \kappa(\rho(\mathbf{r}'))\Delta_{\mathbf{r}}\delta(\mathbf{r} - \mathbf{r}') - \kappa(\rho(\mathbf{r}))\Delta_{\mathbf{r}'}\delta(\mathbf{r} - \mathbf{r}'). \quad (1.57)$$

Integrating against pairs of function  $\phi(\mathbf{r})$  and  $\psi(\mathbf{r}')$  then leads to

$$\int d\mathbf{r}d\mathbf{r}'\mathcal{D}(\mathbf{r}, \mathbf{r}')\phi(\mathbf{r})\psi(\mathbf{r}') = \int d\mathbf{r}\nabla\kappa(\rho(\mathbf{r})) \cdot [\phi(\mathbf{r})\nabla\psi(\mathbf{r}) - \psi(\mathbf{r})\nabla\phi(\mathbf{r})]. \quad (1.58)$$

This vanishes for any  $\rho, \psi, \phi$  if and only if  $\kappa'(\rho) = 0$ . Using the expression (1.56) for  $\kappa$ , this shows that the quasi-local approximation (1.55) admits an equilibrium free energy iff

$$v(\tilde{\rho}) = v_0 \exp[\lambda\tilde{\rho}]. \quad (1.59)$$

This functional form of  $v$  leads to MIPS for  $\lambda < 0$  and to a free energy

$$\mathcal{F} = \int d\mathbf{r} \left[ \rho(\mathbf{r}) \ln \rho(\mathbf{r}) + \frac{\lambda}{2} \rho(\mathbf{r})^2 - \frac{\lambda D}{2\gamma} [\nabla \rho(\mathbf{r})]^2 \right]. \quad (1.60)$$

While interfaces now have a finite cost, the free energy density in Eq. (1.60) is not bounded from below. As  $\rho(\mathbf{r})$  keeps increasing locally,  $f(\rho(\mathbf{r}))$  becomes arbitrarily negative: a macroscopic fraction of the mass thus tends to accumulate in a finite portion of space. For the functional

form (1.59), our equilibrium theory thus predicts — to the order (1.55) in the gradient expansion — a condensation transition instead of a phase separation between finite densities.

For more general forms of  $v(\rho)$ , the system is endowed with a *bona fide* nonequilibrium dynamics. A local approximation to the chemical potential may qualitatively explain the occurrence of MIPS, but more general properties, such as the existence of state functions or simply coexisting densities appear out of reach.

### A generalized equilibrium theory at mean-field level

Progress can however be made at mean-field level. Introducing  $\bar{\rho} = \langle \rho \rangle$  and making the local mean-field approximation  $\langle g(\bar{\rho}) \rangle = g(\langle \bar{\rho} \rangle)$  for any function  $g$ , the dynamics of  $\bar{\rho}$  can be obtained as:

$$\partial_t \bar{\rho}(\mathbf{r}, t) = \nabla \cdot [M \nabla \bar{\mu}] \quad \text{with} \quad \bar{\mu} = \log[\bar{\rho} v(\bar{\rho})] - \kappa(\bar{\rho}) \Delta \bar{\rho}. \quad (1.61)$$

While  $\bar{\mu}$  cannot be written as the functional derivative of a functional  $\mathcal{F}$  with respect to  $\rho$ , we can look for a change of variable  $R(\bar{\rho})$  such that

$$\bar{\mu} = \frac{\delta \mathcal{H}}{\delta R(\bar{\rho})}. \quad (1.62)$$

Remarkably, defining  $R$  from

$$R'(\bar{\rho}) = -\frac{1}{\kappa(\bar{\rho})} \quad (1.63)$$

indeed leads to Eq. (1.62), where the generalized free energy  $\mathcal{H}$  is given by<sup>6,35</sup>

$$\mathcal{H} = \int d\mathbf{r} \left[ \phi(R) + \frac{\kappa}{2R'(\bar{\rho})} (\nabla R)^2 \right] \quad \text{where} \quad \frac{d\phi(R)}{dR} = \ln[\bar{\rho} v(\bar{\rho})]. \quad (1.64)$$

Note that we here provide directly the change of variable  $R(\bar{\rho})$  that allows writing Eq. (1.62). This change of variable can actually be constructed systematically by rewriting Eq. (1.43) using functional derivatives with respect to  $R(\mathbf{r}')$  and  $R(\mathbf{r})$ , and by requiring the corresponding distribution  $D$  to vanish.<sup>36</sup>

Once we have derived the effective free energy (1.64), constructing the steady-state profiles  $R(\mathbf{r})$  amounts to an equilibrium problem. For instance, the coexisting generalized densities  $R_g$  and  $R_\ell$  can be obtained from a common tangent construction on  $\phi(R)$ . Inverting  $R(\rho)$  then leads to the values of the gas and liquid binodals  $\rho_g$  and  $\rho_\ell$ . This procedure is illustrated in Fig. 1.7 where we compare with results from microscopic simulations using a self-propulsion velocity given by

$$v(\tilde{\rho}) = v_g + \frac{v_\ell - v_g}{2} \left[ 1 + \tanh \left( 2 \frac{\tilde{\rho}}{\rho_m} - 2 \right) \right] \quad (1.65)$$

and a coarse-graining kernel

$$G(\mathbf{r}) = \frac{\Theta(r_0 - |\mathbf{r}|)}{Z} \exp \left( -\frac{r_0^2}{r_0^2 - r^2} \right), \quad (1.66)$$

where  $\Theta$  is the Heaviside function.

The binodals predicted by the local, equilibrium theory correspond to the solid black line in Fig. 1.7b and clearly fail to describe the microscopic simulations given by the symbols. On the contrary, the procedure described above, summarized in Fig. 1.7a, lead to the solid red lines, which agree very well with the microscopic simulations.

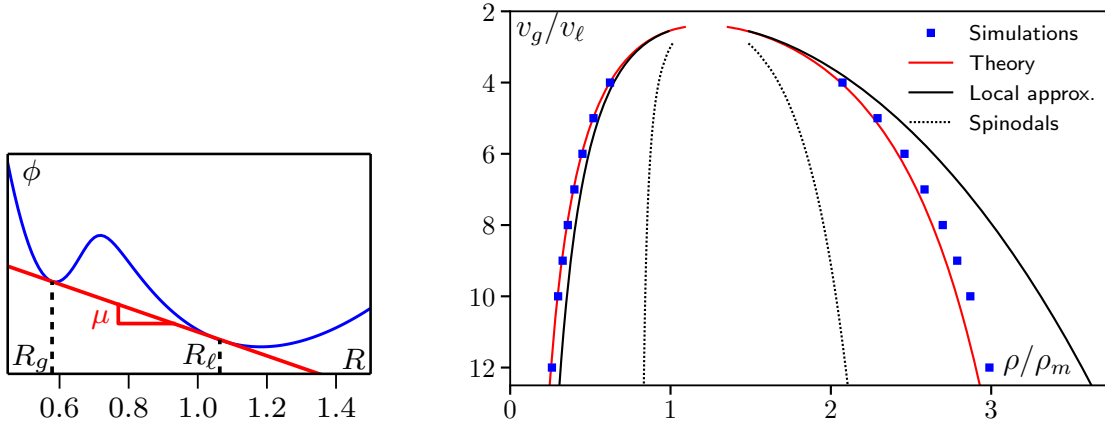


Figure 1.7: (a) The binodals are computed through a common tangent construction on the generalized free energy defined in Eq. (1.64). (b) Comparison between the binodals measured in simulations of RTPs in 2d and the binodals predicted by the local approximation (plain black line) and the mean-field non-local theory (red line). Note that we do not expect the latter to be a good approximation close to the critical point where fluctuations are crucial and at high  $v_0$  because gradients become steeper and higher-order gradient terms become important. Parameters: the self-propulsion given by Eq. (1.65) with  $\rho_m = 200$ ,  $v_\ell = 5$ ,  $\tau = 1$  and system size  $50 \times 50$ .

### 1.6.3 The fully non-local theory

Finally, a natural question is whether a mapping to equilibrium exists for the general form (1.45), where  $v$  is a functional of the non-local effective density  $\tilde{\rho}(\mathbf{r}) = \int d\mathbf{r}' G(\mathbf{r} - \mathbf{r}') \rho(\mathbf{r}')$ . In such a case, the distribution  $\mathcal{D}$  is equal to

$$\mathcal{D}(\mathbf{r}, \mathbf{r}') = \frac{1}{v(\mathbf{r}, [\rho])} \frac{\delta v(\mathbf{r}, [\rho])}{\delta \rho(\mathbf{r}')} - \frac{1}{v(\mathbf{r}', [\rho])} \frac{\delta v(\mathbf{r}', [\rho])}{\delta \rho(\mathbf{r})}. \quad (1.67)$$

Using that Eq. (1.45) can be written as  $v(\mathbf{r}, [\rho]) = v[\int d\mathbf{r}'' G(\mathbf{r} - \mathbf{r}'') \rho(\mathbf{r}'')]$ , one gets

$$\frac{\delta v(\mathbf{r}, [\rho])}{\delta \rho(\mathbf{r}')} = v'(\mathbf{r}, [\rho]) \int d\mathbf{r}'' G(\mathbf{r} - \mathbf{r}'') \frac{\delta \rho(\mathbf{r}'')}{\delta \rho(\mathbf{r}')}, \quad (1.68)$$

where  $v'(\mathbf{r}, [\rho]) = \frac{d}{d\tilde{\rho}} v(\tilde{\rho})$ . In turns, this leads to

$$\mathcal{D}(\mathbf{r}, \mathbf{r}') = \frac{v'(\mathbf{r}, [\rho])}{v(\mathbf{r}, [\rho])} G(\mathbf{r} - \mathbf{r}') - \frac{v'(\mathbf{r}', [\rho])}{v(\mathbf{r}', [\rho])} G(\mathbf{r}' - \mathbf{r}). \quad (1.69)$$

Given the isotropy of  $G$ , the solution to Eq. (1.69) is

$$\frac{v'(\mathbf{r}', [\rho])}{v(\mathbf{r}', [\rho])} = \lambda \in \mathbb{R} \quad \text{so that} \quad v(\mathbf{r}, [\rho]) = v_0 e^{\lambda \int d\mathbf{r}' G(\mathbf{r} - \mathbf{r}') \rho(\mathbf{r}')}. \quad (1.70)$$

The sole function  $v(\tilde{\rho})$  leading to an equilibrium mapping is thus the exponential function.<sup>5,37</sup> In this case, the free energy  $\mathcal{F}$  is given by

$$\mathcal{F} = \int d\mathbf{r} \rho(\mathbf{r}) \ln[\rho(\mathbf{r})] + \frac{1}{2} \lambda \int d\mathbf{r} d\mathbf{r}' \rho(\mathbf{r}) \rho(\mathbf{r}') G(\mathbf{r} - \mathbf{r}'). \quad (1.71)$$

The dynamics of  $N$  RTPs interacting via quorum-sensing interactions and a density-dependent swim speed that varies exponentially thus map, at the coarse-grained level, to that of  $N$  equilibrium Brownian colloids whose interaction potential is given by  $\lambda G(\mathbf{r})$ . If  $\lambda G(\mathbf{r})$  corresponds, say, to a repulsive hard core and attractive tails, then MIPS in QSAPs is mapped exactly to the liquid-gas phase separation observed for attractive colloidal particles.

The mapping discussed in this section belongs to a larger class of mappings between active and passive particles<sup>33</sup> that also exist for tactic dynamics. The mapping (1.71) does not simply map MIPS onto the phase-separation observed for passive particles, it says that the full range of phenomena observed for interacting passive particles can be observed for active ones, upon a highly counter-intuitive mapping between the kernel  $G$  and the interaction potential of passive particles.

#### 1.6.4 QSAPs: conclusion

We close here our discussion of active particles interacting via quorum-sensing interactions, which is the model for which MIPS is best understood. Depending on the question asked, various levels of description offer answers of increasing complexities. First, a simple heuristic argument, detailed in Section 1.3, explains the instability mechanism leading to MIPS. Then, a qualitative mapping to equilibrium models, discussed in Section 1.6.1, establishes an unexpected similarity between motility regulation in active matter and pairwise forces in equilibrium systems. This mapping is shown to break down at the first non-trivial order in a gradient expansion. Then a generalized free energy can be constructed at mean-field level, whose predictive power was demonstrated numerically. Note that, in addition to the coexisting densities discussed so far, this generalized free energy allows tackling a broader set of questions. For instance, it allows demonstrating that the thermodynamic pressure  $p_T$  is not a state function and instead suggests  $p_R = R \frac{d\phi}{dR} - \phi$  as a (mean-field) alternate. The latter can be shown, for instance, to govern Laplace pressure jumps that account for finite-size corrections to coexisting binodals in finite systems.<sup>35</sup>

More generally, the exact mapping between active and passive systems established at the fluctuating-hydrodynamics level in Section 1.6.3 paves the way to a thermodynamics of QSAPs. It comes with restrictions and cannot encompass all scalar active matter systems, but it offers a route to thermodynamics where everything is under control analytically.

In the next section, we briefly discuss the case of active particles interacting via pairwise forces, highlighting similarities and differences with the case of QSAPs.

### 1.7 Active particles interacting via pairwise forces

As discussed in the introduction, another important class of systems that undergo motility-induced phase separation consists in self-propelled particles interacting via repulsive forces

(PFAPs). Their dynamics can typically be written as

$$\dot{\mathbf{r}}_i = v_0 \mathbf{u}_i - u \sum_{j \neq i} \nabla_i V(\mathbf{r}_i - \mathbf{r}_j), \quad (1.72)$$

where  $v_0$  is the single-particle propulsion speed,  $\mathbf{u}_i$  the orientation of particle  $i$ ,  $u$  the particle mobility, and  $V$  an interaction potential. MIPS has been reported for a variety of repulsive potentials such as harmonic spheres,<sup>24</sup> the Yukawa potential<sup>11</sup> or the Week-Chandler-Andersen potential.<sup>38</sup> While most studies have focused on the 2D case, MIPS has also been reported in three dimensions<sup>39–41</sup> and studied analytically in the limit of infinite space dimensions.<sup>42</sup>

### 1.7.1 A quorum-sensing approximation

Let us now illustrate how the emergence of MIPS in PFAPs can easily be understood using a local mean-field theory. Consider the dynamics (1.72) for particle  $i$ . Introducing the projector on the orientation  $\mathbf{u}_i$ , whose components are given by  $u_i^\alpha u_i^\beta$ , the dynamics can be rewritten as

$$\dot{\mathbf{r}}_i = v_{i,\text{eff}} \mathbf{u}_i + \boldsymbol{\xi}_i, \quad (1.73)$$

where we have introduced the effective speed  $v_{i,\text{eff}}$  and the ‘noise’  $\boldsymbol{\xi}_i$ , defined by

$$\boldsymbol{\xi}_i \equiv -u \sum_{j \neq i} (1 - \mathbf{u}_i \mathbf{u}_i) \nabla_i V(\mathbf{r}_i - \mathbf{r}_j) \quad \text{and} \quad v_{i,\text{eff}} \equiv v_0 - u \sum_{j \neq i} \mathbf{u}_i \cdot \nabla V(\mathbf{r}_i - \mathbf{r}_j). \quad (1.74)$$

Equations (1.73) and (1.74) are exact; they simply amount to splitting the forces exerted by the particles  $j \neq i$  on particle  $i$  between a contribution parallel to the orientation  $\mathbf{u}_i$ , which renormalizes  $v_0$  into  $v_{i,\text{eff}}$ , and a contribution orthogonal to  $\mathbf{u}_i$  which we denote  $\boldsymbol{\xi}_i$ .

Let us now employ a local mean-field approximation to get more insight into the behaviors of  $v_{i,\text{eff}}$  and  $\boldsymbol{\xi}_i$ . In a homogeneous phase, the orientation  $\mathbf{u}_i$  is an axis of symmetry of particle  $i$  so that  $\langle \boldsymbol{\xi}_i \rangle_j = 0$ , where  $\langle \dots \rangle_j$  refers to an average over  $\mathbf{r}_j$ , keeping  $\mathbf{r}_i$  and  $\mathbf{u}_i$  fixed. On the contrary, most collisions between particle  $i$  and other particles happen when the latter are ahead of particle  $i$ .<sup>43</sup> This can be easily understood by considering the situation in which you are running, say, to catch a train: most of the time, you will collide with people ahead of you, not behind you, especially when everyone is running in random directions. The result is that  $\delta v_i \equiv -u \langle \sum_{j \neq i} \mathbf{u}_i \cdot \nabla V(\mathbf{r}_i - \mathbf{r}_j) \rangle_j$  is negative: repulsive forces oppose self-propulsion. In the low-density limit, where particles are weakly correlated,  $\delta v$  is simply proportional to the number of particles  $j$  with which particle  $i$  interact, and thus to the local density. Furthermore,  $-\nabla V$  is of the order of the typical force to stall a particle, and thus  $|u \nabla V| \simeq v_0$ . Overall,  $\delta v_i \propto \rho(\mathbf{r}_i) v_0$ . Introducing a proportionality constant  $1/\rho^*$ , this leads to an average propulsion speed that scales as

$$v_{\text{eff}}(\mathbf{r}_i) \equiv \langle v_{i,\text{eff}} \rangle = v_0 [1 - \rho(\mathbf{r}_i)/\rho^*], \quad (1.75)$$

where  $\rho^*$  is *a priori* unknown and has the dimension of a density. This linear scaling has indeed been measured in simulations<sup>24</sup> and derived analytically in infinite dimensions.<sup>42</sup>

Given the above discussion, it is tempting to approximate PFAPs by QSAPs whose self-propulsion speeds would be given by Eq. (1.75).<sup>24,43,44</sup> An appealing feature of this approximation is that it offers a simple mechanism accounting for MIPS: for QSAPs, the criterion (1.7)

applied to the self-propulsion speed (1.75) predicts a linear instability leading to MIPS whenever

$$\rho_0 > \rho^*/2. \quad (1.76)$$

This quorum-sensing approximation however suffers from important limitations. First, it predicts that the chemical potential  $\mu = \ln[\rho v_{\text{eff}}(\rho)]$  should be equal in coexisting phases, which is not verified numerically, as we discuss below. Then, the instability criterion (1.76) is independent from  $v_0$ . It thus predicts a phase separation for arbitrarily small self-propulsion speeds  $v_0$ . This, again, contradicts numerical results, which show that the run-length  $v_0/D_r$  has to be larger than  $\sim 15$  particle size  $r_0$  (see Fig. 1.1). Finally, the QSAPs approximation predicts a Laplace-pressure jump in finite-sized droplets coexisting with a gaseous phase that has an opposite sign with respect to the one measured for PFAPs.<sup>35</sup> For all these reasons, an alternate route is preferable to study the MIPS observed for PFAPs.

## 1.7.2 The stress tensor of PFAPs

We now briefly present the path laid out in<sup>8,9,35</sup> for the case of ABPs. Let us denote  $\hat{\rho}(\mathbf{r}) = \sum_{i=1}^N \delta(\mathbf{r} - \mathbf{r}_i)$  the instantaneous, stochastic density field and  $\rho(\mathbf{r}) = \langle \hat{\rho}(\mathbf{r}) \rangle$  its average over realizations of the active dynamics of  $\mathbf{u}_i(t)$ . Using the chain rule, one gets for the dynamics of  $\rho(\mathbf{r}, t)$

$$\partial_t \rho(\mathbf{r}, t) = -\nabla \cdot \mathbf{J}(\mathbf{r}, t), \quad (1.77)$$

where the average density current  $\mathbf{J}$  can be split between active and passive contributions:  $\mathbf{J} = \mathbf{J}^a + \mathbf{J}^p$ , with

$$\mathbf{J}^a(\mathbf{r}, t) = \left\langle \sum_{i=1}^N v_0 \mathbf{u}_i \delta(\mathbf{r} - \mathbf{r}_i) \right\rangle \quad \text{and} \quad \mathbf{J}^p(\mathbf{r}, t) = -u \int d\mathbf{r}' \langle \rho(\mathbf{r}) \rho(\mathbf{r}') \rangle \nabla V(\mathbf{r} - \mathbf{r}'). \quad (1.78)$$

These two currents account for the displacements of particles due to their self-propulsion and to the pairwise forces, respectively.

Let us first note that  $\mathbf{J}^p$  would also contribute to the current for passive Brownian particles interacting via pairwise forces, although, in this case, the average in Eq. (1.78) would be computed using the equilibrium Boltzmann weight. Despite this difference, we can directly borrow results derived for equilibrium systems by Irving and Kirkwood,<sup>45</sup> who showed that  $\mathbf{J}^p$  can be written as the divergence of a stress tensor:  $\mathbf{J}^p = u \nabla \cdot \boldsymbol{\sigma}^{IK}$  where

$$\sigma_{\alpha\beta}^{IK}(\mathbf{r}) = \frac{1}{2} \int d\mathbf{r}' \left\{ \frac{r'_\alpha r'_\beta}{|\mathbf{r}'|} \frac{dV(|\mathbf{r}'|)}{d|\mathbf{r}'|} \int_0^1 d\lambda \langle \hat{\rho}(\mathbf{r} + (1-\lambda)\mathbf{r}') \hat{\rho}(\mathbf{r} - \lambda\mathbf{r}') \rangle \right\}. \quad (1.79)$$

While Eq. (1.79) is not particularly illuminating, it can be shown<sup>9</sup> that  $\boldsymbol{\sigma}^{IK}$  acquires a simpler meaning in homogeneous systems, where, for instance,  $\sigma_{xx}^{IK}(x, y)$  measures the force density exerted by the particles at  $(x' > x, y')$  on those at  $(x' < x, y)$ .

Up to a factor of  $u$ ,  $\mathbf{J}^a(\mathbf{r})$  measures the density of active forces experienced by the system at position  $\mathbf{r}$ . Using Itô formula, its dynamics can be computed as:

$$\partial_t \mathbf{J}^a = \left\langle \sum_{i=1}^N v_0 \dot{\mathbf{u}}_i \delta(\mathbf{r} - \mathbf{r}_i) \right\rangle - \nabla_{\mathbf{r}} \cdot \left\langle \sum_{i=1}^N \dot{\mathbf{r}}_i v_0 \mathbf{u}_i \delta(\mathbf{r} - \mathbf{r}_i) \right\rangle - D_r \left\langle \sum_{i=1}^N v_0 \mathbf{u}_i \delta(\mathbf{r} - \mathbf{r}_i) \right\rangle, \quad (1.80)$$

In the steady-state,  $\partial_t \mathbf{J}^a$  and  $\langle \dot{\mathbf{u}}_i \rangle$  vanish. Using that the last term of Eq. (1.80) is nothing but  $-D_r \mathbf{J}^a$ , we find:<sup>46</sup>

$$\mathbf{J}^a(\mathbf{r}) = \mathbf{u} \nabla \cdot \boldsymbol{\sigma}^a(\mathbf{r}), \quad \text{where} \quad \boldsymbol{\sigma}^a(\mathbf{r}) = -\left\langle \sum_i \dot{\mathbf{r}}_i \frac{v_0 \mathbf{u}_i}{u D_r} \delta(\mathbf{r} - \mathbf{r}_i) \right\rangle. \quad (1.81)$$

Inspection of Eq. (1.81) shows that the active stress tensor  $\boldsymbol{\sigma}^a$  measures the flux of the so-called ‘active impulse’:<sup>46</sup>

$$\delta \mathbf{p}_i^a = \frac{v_0 \mathbf{u}_i(t)}{u D_r} = \int_t^\infty ds \left\langle \frac{v_0 \mathbf{u}_i(s)}{u} \right\rangle, \quad (1.82)$$

which is nothing but the average momentum an active particle will gain, between  $t$  and the end of times, due to its active force  $v_0 \mathbf{u}_i/u$ .

Together, Eqs. (1.79) and (1.81) show that the total current can be written as the divergence of a generalized stress tensor:

$$\mathbf{J}(\mathbf{r}) = \mathbf{u} \nabla \cdot \boldsymbol{\sigma}(\mathbf{r}) \quad \text{where} \quad \boldsymbol{\sigma}(\mathbf{r}) = \boldsymbol{\sigma}^{IK}(\mathbf{r}) + \boldsymbol{\sigma}^a(\mathbf{r}). \quad (1.83)$$

The mechanical implications of  $\boldsymbol{\sigma}$  become apparent by noting that, in the presence of an external potential  $V_w(\mathbf{r})$ , the current becomes  $\mathbf{J}(\mathbf{r}) = \mathbf{u} \nabla \cdot \boldsymbol{\sigma}(\mathbf{r}) - \rho \nabla V_w(\mathbf{r})$ . When  $V_w$  models a wall localized at  $x = 0$ , which prevents the particles from entering the  $x < 0$  subspace, the mechanical pressure exerted by the active particles on this wall in a flux-free steady state can be measured as<sup>47</sup>

$$P_m = - \int_{-\infty}^{x_b} dx \rho(x, y_b) \partial_x V(x, y_b) = -\sigma_{xx}(x_b), \quad (1.84)$$

where  $(x_b, y_b)$  corresponds to a point deep in the bulk of the system. Like passive particles, ABPs interacting via pairwise forces thus admit a stress tensor whose diagonal components are the opposite of the mechanical pressure exerted by the particles on confining walls.

### 1.7.3 MIPS in PFAPs: A mechanical instability

While the mechanical properties of active particles are a fascinating topic,<sup>9,46–50</sup> we are here interested in the consequences of Eq. (1.83) for MIPS. Note that, so far, everything we have done is exact and we now employ approximations to relate MIPS to the properties of  $\boldsymbol{\sigma}$ . In particular, we assume that  $\boldsymbol{\sigma}$  is well described, in homogeneous systems, by an equation of state  $\boldsymbol{\sigma}(\rho_0)$ . (Remember that the density is the only hydrodynamic field in MIPS.)

Let us first look at the linear stability of a homogeneous profile at density  $\rho_0$  against a fluctuation along the  $x$  axis,  $\delta \rho(\mathbf{r}, t) = \delta \rho_q(t) \cos(qx)$ . The time evolution of  $\delta \rho_q$  is then given by

$$\frac{d}{dt} \delta \rho_q(t) = q^2 u \sigma'_{xx}(\rho_0) \delta \rho_q(t) = -q^2 u P'_m(\rho_0) \delta \rho_q(t), \quad (1.85)$$

where we used Eq. (1.84) to work with the pressure instead of the stress tensor. Much like in a passive system, negative values for  $P'_m(\rho_0)$  signal a mechanical instability. Let us now analyze which contributions to  $P_m(\rho_0)$  can be responsible for such a decrease in mechanical pressure as  $\rho_0$  increases.

The passive part of the stress tensor, which leads to a pressure  $P_m^{IK}(\rho_0)$ , behaves qualitatively as that of a passive system comprising repulsive particles:  $P_m^{IK}(\rho_0)$  is an increasing function

that scales as  $\rho_0^2$  at small densities due to the pairwise nature of the forces and diverges at close packing. Inspection of Eq. (1.79) suggests the following scaling form for  $P_m^{IK}(\rho_0)$ : it is proportional to the typical distance between interacting particles multiplied by the interparticle force, due to the factor  $\frac{r'_\alpha r'_\beta}{|\mathbf{r}'|} \frac{dV(|\mathbf{r}'|)}{d|\mathbf{r}'|}$ , whereas the rest of the expression scales as a density. As argued above, the typical scale of the interparticle forces in MIPS is set by the self-propulsion they oppose:  $\frac{dV(|\mathbf{r}'|)}{d|\mathbf{r}'|}$  is, typically, a stalling force and scales as  $v_0/u$ . The particle size  $r_0$  then sets the scale for the interparticle distance and we find

$$P_m^{IK}(\rho_0) \sim \frac{v_0 r_0}{u} \rho_0 \mathcal{S}\left(\frac{\rho_0}{\rho^*}\right) \quad (1.86)$$

where  $\mathcal{S}$  is a scaling function. At small density, the probability of encounters scale as  $\rho_0^2$  so that  $\mathcal{S}(u) \sim u$  as  $u \rightarrow 0$ .

Using Eq. (1.75), we approximate  $P_m^a(\rho_0) \equiv -\sigma_{xx}^a(\rho_0)$  as<sup>9</sup>

$$P_m^a(\rho_0) \sim \frac{v_0 v_{\text{eff}}}{u D_r} \rho_0 = \frac{v_0^2}{u D_r} \rho_0 \left(1 - \frac{\rho_0}{\rho^*}\right). \quad (1.87)$$

While  $P_m^a(\rho_0)$  is increasing—and hence stabilizing—at small densities, it decreases at larger ones due to the decrease in the effective speed. The active pressure can thus trigger an instability. Note that  $P_m^a(\rho_0) < 0$  amounts to  $\rho > \rho^*/2$ : one recovers the "QSAPs" criterion (1.76). The latter accounts for the instability triggered by the slowing down but is missing the crucial contribution of  $P_m^{IK}$ .

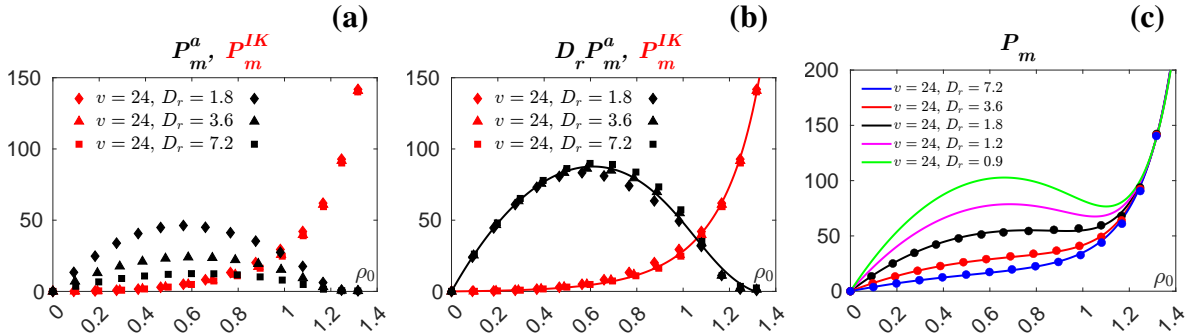


Figure 1.8: Pressure of PFAPs interacting via a repulsive WCA potential. (See<sup>35</sup> for numerical details.) (a)  $P_m^a$  and  $P_m^{IK}$  as the average density  $\rho_0$  is varied, measured for values of  $D_r$  and  $v_0$  leading to homogeneous systems. (b) Rescaling the pressures as  $D_r P_m^a$  and  $P_m^{IK}$  shows the scaling (1.86) and (1.87) of the pressures as  $D_r$  varies to be satisfied. The solid lines show fits to the simulation data, as detailed in.<sup>35</sup> (c) The total pressure  $P_m = P_m^a + P_m^{IK}$  as a function of  $\rho_0$ . The curves for  $D_r = 1.2$  and  $D_r = 0.9$  are obtained by extrapolating the fitted curves in panel b), using the scaling laws predicted in Eqs. (1.86) and (1.87). At a sufficiently small  $D_r$ , and hence a sufficiently large persistence length, the decreasing trend of  $P_m^a$  for  $\rho_0 \geq \rho^*/2$  overcomes the increasing trend of  $P_m^{IK}$ . This leads to a total decreasing pressure,  $P_m^a(\rho_0) < 0$ , and hence a linear instability.

We are now ready to account for the shape of the phase diagram of PFAPs. At small  $v_0$ , the active pressure, which scales as  $v_0^2$ , is negligible. The stabilizing effect of repulsive interactions

dominate and, like in passive systems, they promote a homogeneous phase. At higher speeds, however, the active pressure becomes comparable to the Irving-Kirkwood contribution. When  $\rho_0 \geq \rho^*/2$ , the decreasing trend of  $P_m^a$  may thus overcome the increasing trend of  $P_m^{IK}$ , leading to an overall decreasing pressure. At close packing, the divergence of  $P_m^{IK}$  stabilizes again the system. Balancing Eqs. (1.86) and (1.87) shows that the transition between the two regimes is controlled by the dimensionless number  $v_0/(D_r r_0)$  which compares the particle persistence length to the particle size. In the presence of a finite translational diffusivity  $D_t$ , when  $D_r$  and  $D_t$  are related by Stokes relations, this criterion can be expressed in terms of a Péclet number  $v_0 r_0/D_t$ . However appealing, this choice is unfortunate since the phase diagram of MIPS is barely altered by sending  $D_t$  to zero while maintaining  $D_r$  constant and the physics described above has nothing to do with translational diffusion. The nondimensional persistence length  $v_0/(D_r r_0)$  is thus a better observable to characterize the transition. The scaling laws (1.86) and (1.87) for the ‘passive’ and ‘active’ contributions to the pressure can be tested by measuring  $P_m^a$  and  $P_m^{IK}$  in homogeneous systems at density  $\rho_0$ . We report these measurements in Fig. 1.8 and use them to extrapolate the behaviour of the pressure at larger persistence lengths. Above a ‘critical’ persistence length,  $P_m(\rho_0)$  is non-monotonous, which allows defining a spinodal region where  $P_m'(\rho_0) < 0$  and where a mean-field instability is predicted.

Note that the path laid out above not only explains the instability leading to MIPS for PFAPs, but also how it overcomes the stabilizing effect of repulsive forces, something which could not be discussed within the QSAPs framework. Finally, note that we have obtained a second important result: since  $\mathbf{J} = \mathbf{u}\nabla \cdot \boldsymbol{\sigma}$ , stress tensor and pressure are homogeneous in flux-free steady states. The mechanical pressure thus acts as a state variable in the MIPS exhibited by PFAPs, and it is thus equal in coexisting phases. Figure 1.9 shows an assembly of PFAPs undergoing MIPS. The right panel shows measurements of  $P_m$  and of a putative chemical potential defined as  $\mu \equiv \ln[\rho v_{\text{eff}}(\rho)]$  throughout the system. While  $P_m$  is, as predicted, uniform across the system whereas  $\mu$  is very different between the two phases.

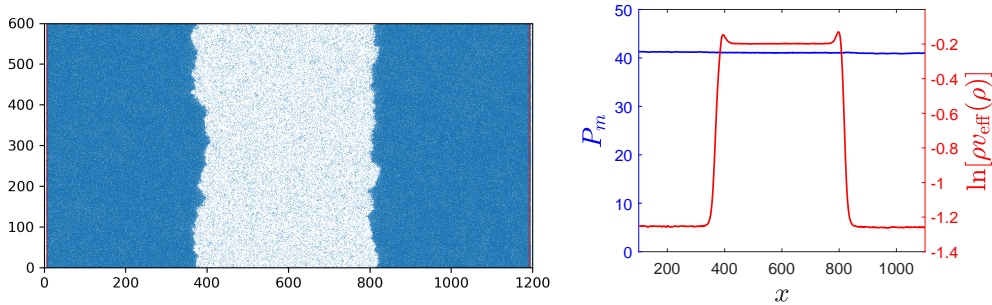


Figure 1.9: **Left:** Self-propelled ABPs interacting via a harmonic repulsive potential and undergoing MIPS. The particles are confined by hard walls at  $x = 8$  and  $x = 1192$  while they experience periodic boundary conditions along the  $y$  direction. **Right:** We measure the pressure  $P_m$  and the chemical potential  $\mu = \ln[\rho v_{\text{eff}}(\rho)]$  in slabs of width  $\Delta x = 2$ . The mechanical pressure, which corresponds to  $-\sigma_{xx}$  is clearly uniform across the system whereas the chemical potential that would be defined using the QSAPs approximation is not.

Before concluding this chapter, we finally discuss in the next section the MIPS observed in lattice models.

## 1.8 MIPS in lattice models

### 1.8.1 Models and phenomenology

Despite being often harder to connect to experimental systems, lattice gases are workhorse models in statistical physics because they allow both for analytical progress and for faster simulations than their off-lattice counterparts. Lattice-based models have been used to model active systems in a variety of settings, in particular to study the transition to collective motion<sup>51–54</sup> and motility-induced phase separation.<sup>55–61</sup> Here, we follow<sup>55</sup> and consider the run-and-tumble dynamics of  $N$  particles on a two-dimensional lattice. Particle  $k$  occupies a site  $\mathbf{i}_k \equiv (i_k, j_k)$  and carries an orientation vector  $\mathbf{u}_k \in \{(\pm 1, 0), (0, \pm 1)\}$ . In the non-interacting case, the particle hops with a constant rate  $p$  from site  $\mathbf{i}_k$  to site  $\mathbf{i}_k + \mathbf{u}_k$  and fully randomizes its orientation at rate  $\alpha$ . Denoting  $a$  the lattice spacing, this leads to a ‘propulsion speed’  $v = pa$ , a persistence length  $\ell_p = pa/\alpha$  and to a large-scale effective diffusivity (See appendix .1):

$$D_0 = \frac{p^2 a^2}{2\alpha} \left( 1 + \frac{\alpha}{2p} \right). \quad (1.88)$$

In the limit  $\ell_p \gg a$ , we thus recover the large-scale diffusivity of an off-lattice RTP in 2D,  $D_0 = v^2/(2\alpha)$ .

To model repulsive forces and steric interactions, the hopping rule can be replaced by a partial exclusion process:<sup>62,63</sup> a particle hops from site  $\mathbf{i}_k$  to site  $\mathbf{i}_k + \mathbf{u}_k$  with a rate

$$W(\mathbf{i}_k \rightarrow \mathbf{i}_k + \mathbf{u}_k) = p \left( 1 - \frac{n_{\mathbf{i}_k + \mathbf{u}_k}}{n_m} \right) \Theta(n_m - n_{\mathbf{i}_k + \mathbf{u}_k}), \quad (1.89)$$

where  $n_{\mathbf{j}}$  is the total number of particles on site  $\mathbf{j}$  and  $n_m$  the maximal occupancy. Note that this amounts to making self-propulsion depend on density, which thus leads to a discretized version of quorum-sensing interactions. The linear decay (1.89) is, however, reminiscent of the effective self-propulsion speed (1.75) measured in the presence of pairwise forces. MIPS has been reported for such lattice models at large enough  $\ell_p$ .<sup>63</sup> Interestingly, for the very model described above, MIPS also requires  $n_m > 1$ ,<sup>56</sup> a constraint which is released if translational noise is added to the model (for instance in the form of a non-vanishing symmetric transverse hopping rate<sup>58</sup>).

### 1.8.2 Linear instability at mean-field level

To illustrate the power of lattice approaches, we now derive the criterion for linear instability leading to MIPS. To lighten the notations, we consider a one-dimensional lattice. In this case, the linear instability leads to alternating finite-size domains of gas and liquid.<sup>5</sup> The physics of the instability is, however, identical to the one leading to MIPS in higher dimensions.

We first remind the generic expression of the master equation that governs the time evolution of the probability  $P(\mathcal{C}, t)$  to observe a configuration  $\mathcal{C}$  at time  $t$ :

$$\partial_t P(\mathcal{C}, t) = \sum_{\mathcal{C}'} W(\mathcal{C}' \rightarrow \mathcal{C}) P(\mathcal{C}', t) - W(\mathcal{C} \rightarrow \mathcal{C}') P(\mathcal{C}, t), \quad (1.90)$$

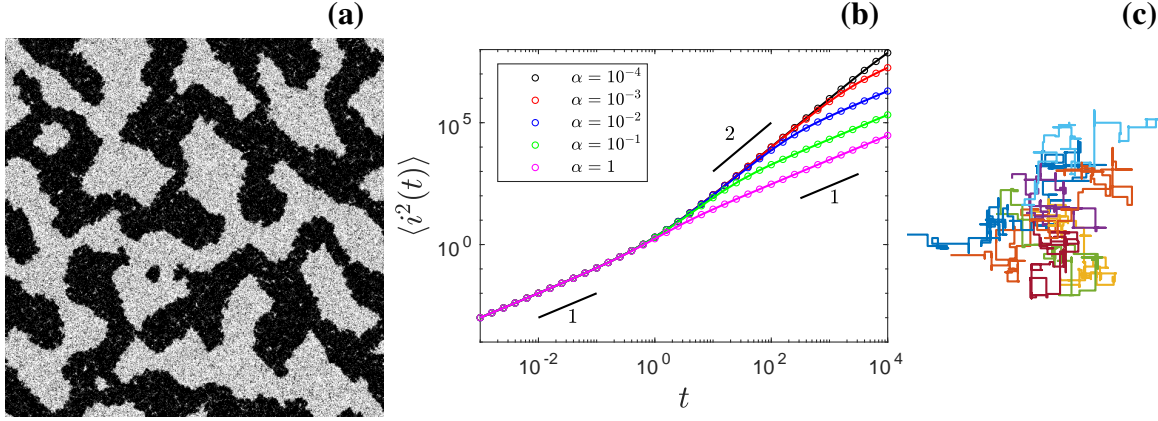


Figure 1.10: MIPS on lattice. **(a)** A snapshot at large time showing the phase separation of RTPs on a 2D square lattice of  $512 \times 512$  sites.  $p = 10$ ,  $\alpha = 1$ ,  $n_m = 5$ . The initial density is  $\langle n \rangle = 3$ . **(b)** Mean squared displacement of a free RTP on a 2D square lattice. Solid lines are from Eq. (124) and circles are from simulations.  $p = 1$ . **(c)** Ten trajectories of non-interacting RTPs starting from the same position on a 2D lattice.  $p = 10$ ,  $\alpha = 1$ .

where  $W(\mathcal{C} \rightarrow \mathcal{C}')$  is the rate at which the system transitions from configuration  $\mathcal{C}$  to configuration  $\mathcal{C}'$ . Consider a generic observable  $O(\mathcal{C})$ . Its average value at time  $t$  is defined as

$$\langle O(t) \rangle \equiv \sum_{\mathcal{C}} O(\mathcal{C}) P(\mathcal{C}, t). \quad (1.91)$$

Using the master equation (1.90), the time evolution of  $\langle O(t) \rangle$  can then be written as

$$\frac{d}{dt} \langle O(t) \rangle = \sum_{\mathcal{C}} \left\{ \sum_{\mathcal{C}'} [O(\mathcal{C}') - O(\mathcal{C})] W(\mathcal{C} \rightarrow \mathcal{C}') \right\} P(\mathcal{C}, t) = \left\langle \sum_{\mathcal{C}'} [O(\mathcal{C}') - O(\mathcal{C})] W(\mathcal{C} \rightarrow \mathcal{C}') \right\rangle_{\mathcal{C}} \quad (1.92)$$

The evolution of the mean of the observable is thus given by its average variation during hops out of configuration  $\mathcal{C}$  weighted by the corresponding rates.

Let us denote  $n_i^\pm$  the numbers of particles at site  $i$  whose orientations are  $\pm e_x$ , respectively. Applying Eq. (1.92) to  $\langle n_i^+ \rangle$  and  $\langle n_i^- \rangle$  leads to

$$\partial_t \langle n_i^+(t) \rangle = \left\langle p n_{i-1}^+ \left(1 - \frac{n_i}{n_m}\right) - p n_i^+ \left(1 - \frac{n_{i+1}}{n_m}\right) + \frac{\alpha}{2} n_i^- - \frac{\alpha}{2} n_i^+ \right\rangle \quad (1.93)$$

$$\partial_t \langle n_i^-(t) \rangle = \left\langle p n_{i+1}^- \left(1 - \frac{n_i}{n_m}\right) - p n_i^- \left(1 - \frac{n_{i-1}}{n_m}\right) - \frac{\alpha}{2} n_i^- + \frac{\alpha}{2} n_i^+ \right\rangle \quad (1.94)$$

At this stage, the dynamics of the one-point functions  $\rho_i^\pm(t) \equiv \langle n_i^\pm(t) \rangle$  involve two-point functions, such as  $\langle n_i^\pm n_{i+1}^\pm \rangle$ , and are thus not closed. A popular choice is then to take a ‘‘mean-field’’ approximation that amounts to neglecting all correlations and to factorize all averages.<sup>64</sup> Under this approximation, the dynamics of  $\rho_i^\pm(t)$  are closed and given by

$$\partial_t \rho_i^\pm = p \rho_{i\mp 1}^\pm \left(1 - \frac{\rho_i}{n_m}\right) - p \rho_i^\pm \left(1 - \frac{\rho_{i\pm 1}}{n_m}\right) \pm \frac{\alpha}{2} \rho_i^- \mp \frac{\alpha}{2} \rho_i^+ \quad (1.95)$$

To make progress, we assume that  $\rho_i^+$  and  $\rho_i^-$  vary on scales much larger than the lattice spacing  $a$ . (Note that, while this is reasonable when  $\ell_p \gg a$ , the interactions may very well

generate sharp fronts that would not satisfy this hypothesis.) We then introduce the density fields of left- and right-going particles, denoted  $\rho^-(x)$  and  $\rho^+(x)$ , respectively, that interpolate the  $\rho_i^\pm$  and satisfy  $\rho_i^\pm = a\rho^\pm(x = ia)$ . Assuming  $\rho^\pm(x)$  to vary smoothly, we expand  $\rho_{i\pm 1}^\pm$  as

$$\rho_{i\pm 1}^\pm = a\rho^\pm(x) \pm a^2\partial_x\rho^\pm(x) + \frac{a^3}{2}\partial_{xx}\rho^\pm(x). \quad (1.96)$$

We now introduce  $\rho_m = n_m/a$ ,  $\rho(x) = \rho^+(x) + \rho^-(x)$  and  $m(x) = \rho^+(x) - \rho^-(x)$ . Taylor-expanding Eq. (1.95) to second order in gradients yields the following dynamics for the fields  $\rho(x, t)$  and  $m(x, t)$ :

$$\partial_t\rho(x) = -\partial_x\left[pam(x)\left(1 - \frac{\rho(x)}{\rho_m}\right) - \frac{pa^2}{2}\partial_x\rho(x)\right] \quad (1.97)$$

$$\partial_t m(x) = -\alpha m(x) - \partial_x\left[pa\rho(x)\left(1 - \frac{\rho(x)}{\rho_m}\right)\right] + \frac{pa^2}{2}\left[\partial_{xx}m(x)\left(1 - \frac{\rho(x)}{\rho_m}\right) + \frac{m\partial_{xx}\rho(x)}{\rho_m}\right], \quad (1.98)$$

where the time-dependence of the fields has been omitted for concision. We note the presence of a ‘bare’ diffusivity  $pa^2/2$  in the dynamics of  $\rho$  which is nothing but the correction to the large-scale diffusivity (1.88) due to the discreteness of the lattice.

Let us now consider the limit in which  $v = pa$  is kept fixed but the lattice spacing  $a$  is assumed to be very small. The persistence length  $\ell_p = v/\alpha$  is thus large compared to  $a$  and we hope the irregularities due to the lattice to be negligible, so that the model should be as close as possible to a continuous one. Assuming the gradients of  $\rho$  and  $m$  to remain finite, the terms proportional to  $pa^2/2$  are negligible in the small- $a$  limit. The dynamics (1.97) and (1.98) thus reduce to

$$\partial_t\rho(x) = -\partial_x\left[vm(x)\left(1 - \frac{\rho(x)}{\rho_m}\right)\right] \quad (1.99)$$

$$\partial_t m(x) = -\alpha m(x) - \partial_x\left[v\rho(x)\left(1 - \frac{\rho(x)}{\rho_m}\right)\right]. \quad (1.100)$$

As in the Section (1.4.1),  $\rho(x)$  is a conserved field whose relaxation time diverges with the system size. On the contrary, the field  $m(x)$  relaxes on a time-scale of order  $\mathcal{O}(\alpha^{-1})$  towards

$$m(x) = -\partial_x\left[\frac{v}{\alpha}\rho(x)\left(1 - \frac{\rho(x)}{\rho_m}\right)\right]. \quad (1.101)$$

It then follows adiabatically the evolution of  $\rho(x, t)$  on hydrodynamic time scales according to Eq. (1.101). All in all, this yields the following non-linear diffusion equation for  $\rho(x, t)$

$$\partial_t\rho(x, t) = \partial_x[D_{\text{coll}}(\rho(x, t))\partial_x\rho(x, t)] \quad \text{where} \quad D_{\text{coll}} = \frac{v^2}{\alpha}\left(1 - \frac{\rho(x)}{\rho_m}\right)\left(1 - \frac{2\rho(x)}{\rho_m}\right) \quad (1.102)$$

is an effective, collective diffusivity.

The stability of a homogeneous profile at density  $\rho_0$  is now simple to predict: when  $D_{\text{coll}}(\rho_0) > 0$ , fluctuations are damped and the homogeneous phase is linearly stable. All our approximations are self-consistent and the dynamics (1.102) would faithfully describe the large-scale

relaxation of the average density field towards  $\rho_0$ . When  $D_{\text{coll}}(\rho_0) < 0$ , on the contrary, fluctuations are amplified and drive a linear instability. In this case, sharp profiles are expected and the gradient expansion should be extended to higher order to compute the inhomogeneous profiles.

Interestingly, the instability criterion amounts to  $\rho_0 > \rho_m/2$ . Considering that the exclusion rule leads to an effective “velocity”  $v(\rho) = v(1 - \rho/\rho_m)$ , this criterion is equivalent to  $v'(\rho)/v(\rho) < -1/\rho$ . In the limit  $\ell_p \gg a$ , the lattice gas thus gives back, using a much simpler computation, the linear instability criterion (1.54) for QSAPs that we derived in Section 1.6.1.

Progress beyond the linear instability is possible using field-theoretical methods that allow constructing the fluctuating hydrodynamics of lattice gases.<sup>55</sup> As for QSAPs, a mapping to an effective equilibrium dynamics can be constructed and the phase diagram can be predicted, using methods identical to those presented in Section 1.6. Furthermore, exact results can be obtained on the phase diagrams of lattice models<sup>59</sup> using recent results from the mathematical-physics literature.<sup>65</sup> These results are, however, beyond the scope of this Chapter.

Having reviewed the three most important classes of systems in which MIPS has been reported, we now conclude this Chapter with a discussion of what is *not* known about MIPS and list some current exciting topics of research.

## 1.9 Conclusion

Motility-induced phase separation is arguably the simplest non-trivial collective phenomenon experienced by active particles. It is non-trivial because its microscopic roots are very different from what leads to phase separation in equilibrium, and because we do not have any theoretical tools that can *a priori* account for its phenomenology. On the other hand, the sole hydrodynamic field is the density, which makes the system particularly simple to describe at the coarse-grained level. We have here focused on the most established properties of MIPS: the microscopic instability that drives phase separation and the coexisting densities in macroscopic phase-separated systems. Many questions regarding MIPS physics and its interplay with other ingredients frequently encountered in active systems however remain open.

In the simplest setting of scalar active matter, the question of the coarsening dynamics leading to MIPS would deserve a thorough investigation. In particular, some active-matter systems have been shown to admit a negative surface tension.<sup>35,66</sup> At the coarse-grained level, this has been predicted to arrest MIPS or to lead to a coexistence between a gaseous phase and a bubbly liquid.<sup>67</sup> The latter has been observed in microscopic simulations of ABPs and other related models<sup>60,68</sup> although a clear connection between microscopic and macroscopic models is still missing.

Then, the simple models discussed in this review lack many ingredients frequently found in active systems. From phoretic<sup>16</sup> and hydrodynamic<sup>14</sup> interactions to population dynamics<sup>17,18,37</sup> they can lead to strong alterations of MIPS physics. Stepping out of the realm of scalar active matter, the interplay between MIPS and aligning interactions is rich<sup>53,69–72</sup> and calls for deeper investigations.

To finish on a positive note, let us stress that the exact mapping onto passive colloids at the fluctuating-hydrodynamic level discussed in Section 1.6.3 offers an interesting perspective. It indeed suggests that MIPS could be of one the many collective behaviors of active systems that could resemble equilibrium physics but that would emerge from microscopic interactions of

a very different nature from their equilibrium counterparts. Whether this offers a new route to account for phenomena observed in biological systems or a pathway to engineer active materials is an exciting perspective that calls for further studies.

*Acknowledgments.* We thank Alberto Dinelli, Luigi Gentile, Yariv Kafri, Christina Kurtzhaler, Howard Stone, and Sunghan Ro for their useful comments on this chapter.

## References

- [1] P. C. Hohenberg and B. I. Halperin, Theory of dynamic critical phenomena, *Reviews of Modern Physics*, 1977, **49**, 435.
- [2] P. M. Chaikin and T. C. Lubensky, *Principles of condensed matter physics*, Cambridge university press Cambridge, 1995, vol. 10.
- [3] J. O’Byrne, Y. Kafri, J. Tailleur and F. van Wijland, Time-(ir) reversibility in active matter: from micro to macro, *arXiv preprint arXiv:2104.03030*, 2021.
- [4] M. E. Cates and J. Tailleur, Motility-induced phase separation, *Annu. Rev. Condens. Matter Phys.*, 2015, **6**, 219–244.
- [5] J. Tailleur and M. E. Cates, Statistical mechanics of interacting run-and-tumble bacteria, *Physical review letters*, 2008, **100**, 218103.
- [6] A. P. Solon, J. Stenhammar, M. E. Cates, Y. Kafri and J. Tailleur, Generalized thermodynamics of phase equilibria in scalar active matter, *Phys. Rev. E*, 2018, **97**, 020602.
- [7] G. Szamel, Self-propelled particle in an external potential: Existence of an effective temperature, *Physical Review E*, 2014, **90**, 012111.
- [8] D. Martin, J. O’Byrne, M. E. Cates, E. Fodor, C. Nardini, J. Tailleur and F. van Wijland, Statistical mechanics of active Ornstein-Uhlenbeck particles, *Physical Review E*, 2021, **103**, 032607.
- [9] A. P. Solon, J. Stenhammar, R. Wittkowski, M. Kardar, Y. Kafri, M. E. Cates and J. Tailleur, Pressure and phase equilibria in interacting active Brownian spheres, *Physical review letters*, 2015, **114**, 198301.
- [10] T. Bäuerle, A. Fischer, T. Speck and C. Bechinger, Self-organization of active particles by quorum sensing rules, *Nature communications*, 2018, **9**, 1–8.
- [11] I. Buttinoni, J. Bialké, F. Kümmel, H. Löwen, C. Bechinger and T. Speck, Dynamical clustering and phase separation in suspensions of self-propelled colloidal particles, *Physical review letters*, 2013, **110**, 238301.
- [12] M. N. Van Der Linden, L. C. Alexander, D. G. Aarts and O. Dauchot, Interrupted motility induced phase separation in aligning active colloids, *Physical review letters*, 2019, **123**, 098001.

- [13] G. Liu, A. Patch, F. Bahar, D. Yllanes, R. D. Welch, M. C. Marchetti, S. Thutupalli and J. W. Shaevitz, Self-Driven Phase Transitions Drive *Myxococcus xanthus* Fruiting Body Formation, *Physical review letters*, 2019, **122**, 248102.
- [14] R. Matas-Navarro, R. Golestanian, T. B. Liverpool and S. M. Fielding, Hydrodynamic suppression of phase separation in active suspensions, *Physical Review E*, 2014, **90**, 032304.
- [15] A. Zöttl and H. Stark, Hydrodynamics determines collective motion and phase behavior of active colloids in quasi-two-dimensional confinement, *Physical review letters*, 2014, **112**, 118101.
- [16] O. Pohl and H. Stark, Dynamic clustering and chemotactic collapse of self-phoretic active particles, *Physical review letters*, 2014, **112**, 238303.
- [17] C. Liu, X. Fu, L. Liu, X. Ren, C. K. Chau, S. Li, L. Xiang, H. Zeng, G. Chen and L.-H. Tang, Sequential establishment of stripe patterns in an expanding cell population, *Science*, 2011, **334**, 238–241.
- [18] M. E. Cates, D. Marenduzzo, I. Pagonabarraga and J. Tailleur, Arrested phase separation in reproducing bacteria creates a generic route to pattern formation, *Proceedings of the National Academy of Sciences*, 2010, **107**, 11715–11720.
- [19] I. Theurkauff, C. Cottin-Bizonne, J. Palacci, C. Ybert and L. Bocquet, Dynamic clustering in active colloidal suspensions with chemical signaling, *Physical review letters*, 2012, **108**, 268303.
- [20] J. Palacci, S. Sacanna, A. P. Steinberg, D. J. Pine and P. M. Chaikin, Living crystals of light-activated colloidal surfers, *Science*, 2013, **339**, 936–940.
- [21] F. Ginot, I. Theurkauff, F. Detcheverry, C. Ybert and C. Cottin-Bizonne, Aggregation-fragmentation and individual dynamics of active clusters, *Nature communications*, 2018, **9**, 1–9.
- [22] J. Arlt, V. A. Martinez, A. Dawson, T. Pilizota and W. C. Poon, Painting with light-powered bacteria, *Nature communications*, 2018, **9**, 1–7.
- [23] G. Frangipane, D. Dell’Arciprete, S. Petracchini, C. Maggi, F. Saglimbeni, S. Bianchi, G. Vizsnyiczai, M. L. Bernardini and R. Di Leonardo, Dynamic density shaping of photokinetic *E. coli*, *Elife*, 2018, **7**, e36608.
- [24] Y. Fily and M. C. Marchetti, Athermal phase separation of self-propelled particles with no alignment, *Physical review letters*, 2012, **108**, 235702.
- [25] M. E. Cates and J. Tailleur, When are active Brownian particles and run-and-tumble particles equivalent? Consequences for motility-induced phase separation, *EPL (Europhysics Letters)*, 2013, **101**, 20010.
- [26] B. Øksendal, in *Stochastic differential equations*, Springer, 2003, pp. 65–84.

- [27] D. S. Dean, Langevin equation for the density of a system of interacting Langevin processes, *Journal of Physics A: Mathematical and General*, 1996, **29**, L613.
- [28] A. Curatolo, N. Zhou, Y. Zhao, C. Liu, A. Daerr, J. Tailleur and J. Huang, Cooperative pattern formation in multi-component bacterial systems through reciprocal motility regulation, *Nature Physics*, 2020, **16**, 1152–1157.
- [29] H. C. Berg, *E. coli in Motion*, Springer Science & Business Media, 2008.
- [30] L. G. Wilson, V. A. Martinez, J. Schwarz-Linek, J. Tailleur, G. Bryant, P. Pusey and W. C. Poon, Differential dynamic microscopy of bacterial motility, *Physical review letters*, 2011, **106**, 018101.
- [31] J. D. Jackson, *Classical electrodynamics*, Wiley, New York, NY, 3rd edn., 1999.
- [32] A. Solon, M. Cates and J. Tailleur, Active brownian particles and run-and-tumble particles: A comparative study, *The European Physical Journal Special Topics*, 2015, **224**, 1231–1262.
- [33] J. O’Byrne and J. Tailleur, Lamellar to Micellar Phases and Beyond: When Tactic Active Systems Admit Free Energy Functionals, *Physical Review Letters*, 2020, **125**, 208003.
- [34] R. Wittkowski, A. Tiribocchi, J. Stenhammar, R. J. Allen, D. Marenduzzo and M. E. Cates, Scalar  $\phi^4$  field theory for active-particle phase separation, *Nature communications*, 2014, **5**, 1–9.
- [35] A. P. Solon, J. Stenhammar, M. E. Cates, Y. Kafri and J. Tailleur, Generalized thermodynamics of motility-induced phase separation: phase equilibria, Laplace pressure, and change of ensembles, *New Journal of Physics*, 2018, **20**, 075001.
- [36] J. O’Byrne, J. Tailleur, In preparation.
- [37] T. Grafke, M. E. Cates and E. Vanden-Eijnden, Spatiotemporal self-organization of fluctuating bacterial colonies, *Physical review letters*, 2017, **119**, 188003.
- [38] G. S. Redner, M. F. Hagan and A. Baskaran, Structure and dynamics of a phase-separating active colloidal fluid, *Physical review letters*, 2013, **110**, 055701.
- [39] J. Stenhammar, D. Marenduzzo, R. J. Allen and M. E. Cates, Phase behaviour of active Brownian particles: the role of dimensionality, *Soft matter*, 2014, **10**, 1489–1499.
- [40] A. Wysocki, R. G. Winkler and G. Gompper, Cooperative motion of active Brownian spheres in three-dimensional dense suspensions, *EPL (Europhysics Letters)*, 2014, **105**, 48004.
- [41] F. Turci and N. B. Wilding, Phase separation and multibody effects in three-dimensional active brownian particles, *Physical Review Letters*, 2021, **126**, 038002.
- [42] T. A. de Pirey, G. Lozano and F. van Wijland, Active hard spheres in infinitely many dimensions, *Physical review letters*, 2019, **123**, 260602.

- [43] J. Bialké, H. Löwen and T. Speck, Microscopic theory for the phase separation of self-propelled repulsive disks, *EPL (Europhysics Letters)*, 2013, **103**, 30008.
- [44] J. Stenhammar, A. Tiribocchi, R. J. Allen, D. Marenduzzo and M. E. Cates, Continuum theory of phase separation kinetics for active Brownian particles, *Physical review letters*, 2013, **111**, 145702.
- [45] J. Irving and J. G. Kirkwood, The statistical mechanical theory of transport processes. IV. The equations of hydrodynamics, *The Journal of chemical physics*, 1950, **18**, 817–829.
- [46] Y. Fily, Y. Kafri, A. P. Solon, J. Tailleur and A. Turner, Mechanical pressure and momentum conservation in dry active matter, *Journal of Physics A: Mathematical and Theoretical*, 2017, **51**, 044003.
- [47] A. P. Solon, Y. Fily, A. Baskaran, M. E. Cates, Y. Kafri, M. Kardar and J. Tailleur, Pressure is not a state function for generic active fluids, *Nature Physics*, 2015, **11**, 673–678.
- [48] S. C. Takatori, W. Yan and J. F. Brady, Swim pressure: stress generation in active matter, *Physical review letters*, 2014, **113**, 028103.
- [49] X. Yang, M. L. Manning and M. C. Marchetti, Aggregation and segregation of confined active particles, *Soft matter*, 2014, **10**, 6477–6484.
- [50] Y. B. Dor, Y. Kafri and J. Tailleur, Forces in dry active matter, *arXiv preprint arXiv:1811.08829*, 2018.
- [51] Z. Csahók and T. Vicsek, Lattice-gas model for collective biological motion, *Physical Review E*, 1995, **52**, 5297.
- [52] O. O’Loan and M. Evans, Alternating steady state in one-dimensional flocking, *Journal of Physics A: Mathematical and General*, 1999, **32**, L99.
- [53] F. Peruani, T. Klaus, A. Deutsch and A. Voss-Boehme, Traffic jams, gliders, and bands in the quest for collective motion of self-propelled particles, *Physical Review Letters*, 2011, **106**, 128101.
- [54] A. Solon and J. Tailleur, Revisiting the flocking transition using active spins, *Physical review letters*, 2013, **111**, 078101.
- [55] A. G. Thompson, J. Tailleur, M. E. Cates and R. A. Blythe, Lattice models of nonequilibrium bacterial dynamics, *Journal of Statistical Mechanics: Theory and Experiment*, 2011, **2011**, P02029.
- [56] R. Soto and R. Golestanian, Run-and-tumble dynamics in a crowded environment: Persistent exclusion process for swimmers, *Physical Review E*, 2014, **89**, 012706.
- [57] A. Manacorda and A. Puglisi, Lattice model to derive the fluctuating hydrodynamics of active particles with inertia, *Physical review letters*, 2017, **119**, 208003.

- [58] S. Whitelam, K. Klymko and D. Mandal, Phase separation and large deviations of lattice active matter, *The Journal of chemical physics*, 2018, **148**, 154902.
- [59] M. Kourbane-Houssene, C. Erignoux, T. Bodineau and J. Tailleur, Exact hydrodynamic description of active lattice gases, *Physical review letters*, 2018, **120**, 268003.
- [60] X.-q. Shi, G. Fausti, H. Chaté, C. Nardini and A. Solon, Self-Organized Critical Coexistence Phase in Repulsive Active Particles, *Physical Review Letters*, 2020, **125**, 168001.
- [61] S. Ro, Y. Kafri, M. Kardar and J. Tailleur, Disorder-induced long-ranged correlations in scalar active matter, *Physical Review Letters*, 2021, **126**, 048003.
- [62] G. Schütz and S. Sandow, Non-Abelian symmetries of stochastic processes: Derivation of correlation functions for random-vertex models and disordered-interacting-particle systems, *Physical Review E*, 1994, **49**, 2726.
- [63] J. Tailleur, J. Kurchan and V. Lecomte, Mapping out-of-equilibrium into equilibrium in one-dimensional transport models, *Journal of Physics A: Mathematical and Theoretical*, 2008, **41**, 505001.
- [64] R. A. Blythe and M. R. Evans, Nonequilibrium steady states of matrix-product form: a solver's guide, *Journal of Physics A: Mathematical and Theoretical*, 2007, **40**, R333.
- [65] C. Erignoux, Hydrodynamic limit of boundary driven exclusion processes with nonreversible boundary dynamics, *Journal of Statistical Physics*, 2018, **172**, 1327–1357.
- [66] J. Bialké, J. T. Siebert, H. Löwen and T. Speck, Negative interfacial tension in phase-separated active Brownian particles, *Physical review letters*, 2015, **115**, 098301.
- [67] E. Tjhung, C. Nardini and M. E. Cates, Cluster phases and bubbly phase separation in active fluids: reversal of the Ostwald process, *Physical Review X*, 2018, **8**, 031080.
- [68] C. B. Caporusso, P. Digregorio, D. Levis, L. F. Cugliandolo and G. Gonnella, Motility-Induced Microphase and Macrophase Separation in a Two-Dimensional Active Brownian Particle System, *Physical Review Letters*, 2020, **125**, 178004.
- [69] F. Farrell, M. Marchetti, D. Marenduzzo and J. Tailleur, Pattern formation in self-propelled particles with density-dependent motility, *Physical review letters*, 2012, **108**, 248101.
- [70] E. Sese-Sansa, I. Pagonabarraga and D. Levis, Velocity alignment promotes motility-induced phase separation, *EPL (Europhysics Letters)*, 2018, **124**, 30004.
- [71] X.-q. Shi and H. Chaté, Self-propelled rods: Linking alignment-dominated and repulsion-dominated active matter, *arXiv preprint arXiv:1807.00294*, 2018.
- [72] D. Geyer, D. Martin, J. Tailleur and D. Bartolo, Freezing a flock: Motility-induced phase separation in polar active liquids, *Physical Review X*, 2019, **9**, 031043.

## .1 Mean squared displacement of an RTP on lattice

### .1.1 Diffusivity

Let us first provide a simple derivation of the large-scale diffusivity (1.88). We consider a single run-and-tumble particle on a  $d$ -dimensional square lattice. In the unit of lattice spacing  $a$ , we denote the displacement of the  $j$ -th run as  $\mathbf{s}_j$ . The total displacement  $\Delta \mathbf{i}$  at time  $t$  is, by definition,

$$\Delta \mathbf{i}(t) = \sum_{j=1}^{n(t)} \mathbf{s}_j, \quad (103)$$

where  $n(t)$  is the number of runs until time  $t$ . The mean squared displacement (MSD) at time  $t$  is then given by

$$\langle \Delta i^2(t) \rangle = \left\langle \sum_{j=1}^{n(t)} s_j^2 \right\rangle + 2 \left\langle \sum_{j < k} \mathbf{s}_j \cdot \mathbf{s}_k \right\rangle. \quad (104)$$

Note that both  $n(t)$  and the  $\mathbf{s}_i$ 's are random variables.

Since we consider isotropic tumbles,  $\langle \mathbf{s}_j \rangle = 0$  and the displacements during different runs are independent so that, for  $i \neq j$ ,

$$\langle \mathbf{s}_i \cdot \mathbf{s}_j \rangle = \langle \mathbf{s}_i \rangle \cdot \langle \mathbf{s}_j \rangle = 0, \quad (105)$$

and the last term in (104) vanishes.

Since the run lengths are identically distributed, Wald's identity states that, in the large  $t$  limit,

$$\langle \Delta i^2(t) \rangle \underset{t \rightarrow \infty}{\sim} \langle n(t) \rangle \langle s^2 \rangle, \quad (106)$$

where  $\langle s^2 \rangle$  is the second moment of the run length (measured in units of the lattice spacing). The average number of runs is given by  $\langle n(t) \rangle = \alpha t$ . Every time the particle changes configuration, it has a probability  $p/(p + \alpha)$  to hop and a probability  $\alpha/(p + \alpha)$  to tumble. The probability distribution  $P(s)$  that a run corresponds to  $s$  hops is thus given by

$$P(s) = \frac{p^s \alpha}{(p + \alpha)^{s+1}}. \quad (107)$$

Note that the very last run is not necessarily finished at time  $t$ , and is thus not distributed according to Eq. (107). This is why this heuristic calculation applies only in the large-time limit. By direct calculation, Eq. (107) leads to

$$\langle s^2 \rangle = \sum_{s=1}^{\infty} P(s) s^2 = \frac{2p^2 + \alpha p}{\alpha^2}. \quad (108)$$

All in all, we thus find that the late-time MSD satisfies

$$\langle \Delta i^2(t) \rangle \underset{t \rightarrow \infty}{\sim} \langle n(t) \rangle \langle s^2 \rangle = \frac{2p^2 + \alpha p}{\alpha} t. \quad (109)$$

Restoring the unit of length, the diffusivity satisfies  $\langle a^2 \Delta i^2(t) \rangle \sim 2dD_0t$  in the large- $t$  limit so that

$$D_0 = \frac{2p^2 + \alpha p}{2d\alpha} a^2 = \frac{p^2 a^2}{d\alpha} \left( 1 + \frac{\alpha}{2p} \right). \quad (110)$$

Setting  $d = 2$  for a 2D lattice leads to Eq. (1.88).

This heuristic derivation provides an insight into the large-time asymptotic behaviour of the MSD. We note that the term  $\alpha/(2p)$  in the bracket, which is absent in the continuous model, stems from the non-exponential statistics of the run length  $s$ . In the continuous model,  $s$  is exponentially distributed so that  $\langle s^2 \rangle = 2\langle s \rangle^2$ . This is not the case on lattice for finite  $p$  and  $\alpha$ , but Eq. (107) shows that, as  $p \gg \alpha$ ,  $P(s) \sim \frac{\alpha}{p} \exp[-\alpha s/p]$ , which thus leads back to the result of the continuous model in this limit.

## .1.2 Mean-square displacement at all times

We now provide the full expression of the MSD at all times. We consider the probability density  $P(\mathbf{i}, \mathbf{u}, t)$  of finding the particle at site  $\mathbf{i}$  with orientation  $\mathbf{u}$  at time  $t$ , where  $\mathbf{i} = (i_1, i_2, \dots, i_d)$  and  $\mathbf{u}$  is one of the  $2d$  unit vectors  $\mathbf{u}^{(\pm j)}$  with  $j \in \llbracket 1; d \rrbracket$  and  $u_k^{(\pm j)} \equiv \pm \delta_{jk}$ . Since the system is isotropic, we can, without loss of generality, consider only the displacements along the direction  $i_1$ . We denote the corresponding marginal probability densities  $P_{\pm}(i_1, t) = \sum_{i_2, \dots, i_d} P(\mathbf{i}, \mathbf{u}^{(\pm 1)}, t)$  and  $P_0(i_1, t) = \sum_{i_2, \dots, i_d} \sum_{\mathbf{u} \neq \mathbf{u}^{(\pm 1)}} P(\mathbf{i}, \mathbf{u}, t)$ .  $P_+(i_1, t)$  and  $P_-(i_1, t)$  correspond to the particle being in a site  $\mathbf{i}$  whose first component equals  $i_1$ , going towards greater and smaller values of  $i_1$ , respectively.  $P_0$  correspond to the particle going along one of the  $d - 1$  orthogonal directions. The master equations can be written as

$$\frac{\partial}{\partial t} P_{\pm}(i_1, t) = pP_{\pm}(i_1 \mp 1, t) - pP_{\pm}(i_1, t) - \alpha P_{\pm}(i_1, t) + \frac{\alpha}{2d} [P_+(i_1, t) + P_-(i_1, t) + P_0(i_1, t)], \quad (111)$$

$$\frac{\partial}{\partial t} P_0(i_1, t) = -\alpha P_0(i_1, t) + \alpha \frac{2d-2}{2d} [P_+(i_1, t) + P_-(i_1, t) + P_0(i_1, t)]. \quad (112)$$

We introduce the generating functions

$$G_{+,-,0}(z, t) = \sum_{i_1=-\infty}^{\infty} z^{i_1} P_{+,-,0}(i_1, t) \quad \text{and} \quad G(z, t) = G_+ + G_- + G_0. \quad (113)$$

Direct computation shows that  $G'(z=1, t) = \langle i_1(t) \rangle$  and  $G''(z=1, t) = \langle i_1^2(t) \rangle - \langle i_1(t) \rangle^2$ , where the prime denotes a derivative with respect to  $z$ . We consider the initial condition  $i_1(t=0) = 0$  so that the MSD can be obtained from the derivatives of  $G$  as

$$\langle \Delta i_1^2(t) \rangle = G''(1, t) + G'(1, t) \quad (114)$$

Multiplying Eqs. (111) and (112) by  $z^{i_1}$  and summing on  $i_1$ , we find that

$$\frac{\partial}{\partial t} G_+(z, t) = p(z-1)G_+ - \alpha G_+ + \frac{\alpha}{2d} G, \quad (115)$$

$$\frac{\partial}{\partial t} G_-(z, t) = p\left(\frac{1}{z} - 1\right)G_- - \alpha G_- + \frac{\alpha}{2d} G, \quad (116)$$

$$\frac{\partial}{\partial t} G_0(z, t) = -\alpha G_0 + \alpha \frac{(2d-2)}{2d} G, \quad (117)$$

which form a closed set of ordinary differential equations. We consider an isotropic initial condition so that  $P_+(i_1, 0) = P_-(i_1, 0) = \delta_{i_1, 0}/(2d)$ . This directly leads to  $G_+(z, 0) = G_-(z, 0) = 1/(2d)$ ,  $G_0(z, 0) = 1 - 1/d$  and to the vanishing of their derivatives:  $G'_+(z, 0) = G'_-(z, 0) = G'_0(z, 0) = 0$ . Note that normalization of probability imposes  $G(1, t) = 1$ . Furthermore, Eqs. (115)-(117) at  $z = 1$  leads to

$$G_+(1, t) = G_-(1, t) = \frac{1}{2d}; \quad G_0(1, t) = 1 - \frac{1}{d}. \quad (118)$$

To calculate  $G''(1, t)$ , we take twice the derivative with respect to  $z$  of both sides of Eqs. (115)-(117) and set  $z = 1$ . The first derivative yields

$$\frac{\partial}{\partial t} G'_+(1, t) = pG_+(1, t) - \alpha G'_+(1, t) + \frac{\alpha}{2d} G'(1, t), \quad (119)$$

$$\frac{\partial}{\partial t} G'_-(1, t) = -pG_-(1, t) - \alpha G'_-(1, t) + \frac{\alpha}{2d} G'(1, t), \quad (120)$$

$$\frac{\partial}{\partial t} G'_0(1, t) = -\alpha G'_0(1, t) + \alpha \frac{2d-2}{2d} G'(1, t). \quad (121)$$

By symmetry,  $G'(1, t) = \langle i_1(t) \rangle = 0$ . Using Eq.(118), we can solve Eqs (119)- (121) to get

$$G'_+(1, t) = -G'_-(1, t) = \frac{p}{2d\alpha} [1 - e^{-\alpha t}], \quad G'_0(1, t) = 0. \quad (122)$$

The second derivative with respect to  $z$  then gives, for  $z = 1$ ,

$$\frac{\partial}{\partial t} G''(1, t) = 2p[G'_+(1, t) - G'_-(1, t) + G_-(1, t)] = \frac{2p^2}{d\alpha} [1 - \exp(-\alpha t)] + \frac{p}{d}. \quad (123)$$

Using the initial condition  $G''(1, 0) = 0$ , the integration of Eq. (123) leads to

$$\langle \Delta i_1^2(t) \rangle = G''(1, t) + G'(1, t) = \frac{2p^2}{d\alpha} \left( 1 + \frac{\alpha}{2p} \right) t + \frac{2p^2}{d\alpha^2} [\exp(-\alpha t) - 1]. \quad (124)$$

Equation (124) predicts the MSD at all times of an RTP on a  $d$ -dimensional lattice. Note that, as  $t \rightarrow 0$ , the motion of the particle is diffusive, with a diffusion constant  $p/(2d)$ . This diffusive regime stems from the stochasticity of the hops along the lattice. As  $t$  increases, the dynamics transitions into a ballistic regime, typical of an active particle. At large times, when  $t \gg \alpha^{-1}$ , the tumbles make the large-scale dynamics diffusive. We then recover Eq. (109), using  $\langle \Delta i^2(t) \rangle = d \langle \Delta i_1^2(t) \rangle$ .